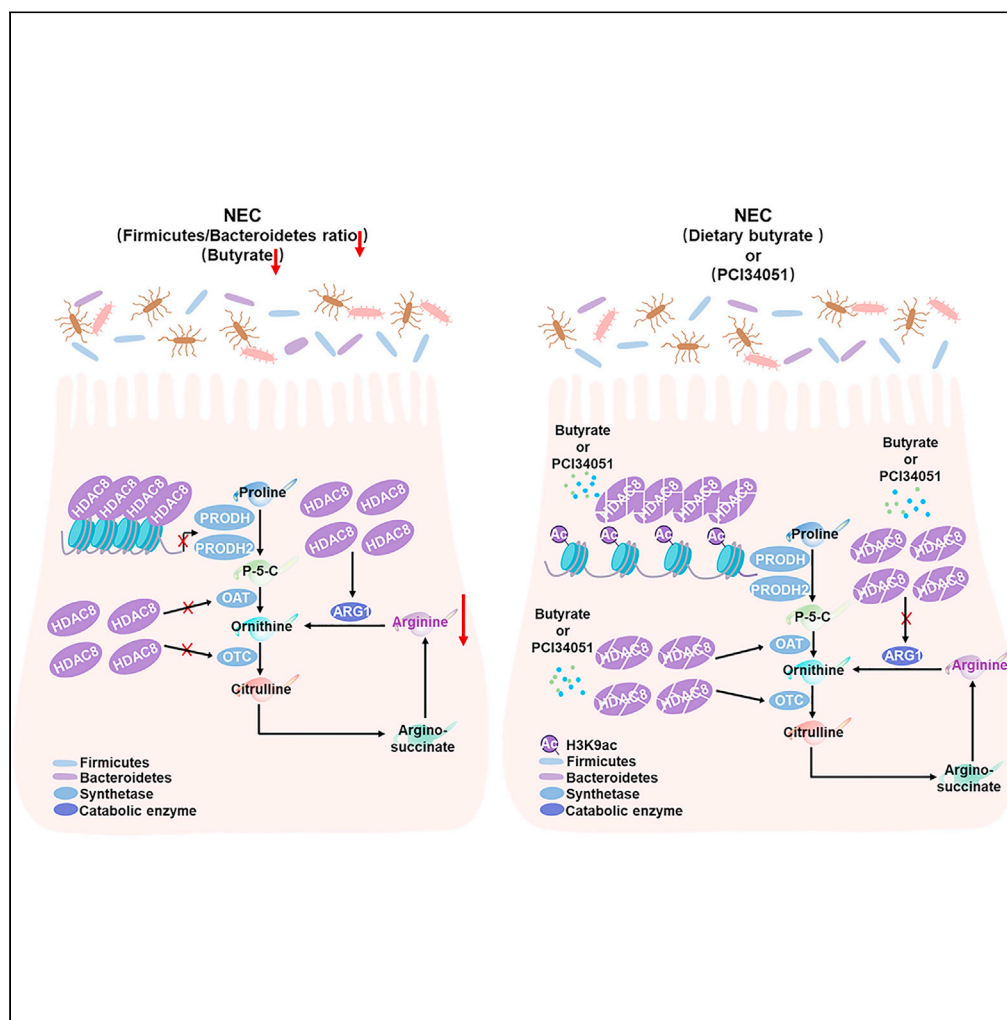


Article

Elevated expression of histone deacetylase HDAC8 suppresses arginine-proline metabolism in necrotizing enterocolitis



Ting Guo,
Shaohua Hu,
Weijue Xu, ...,
Faling Chen,
Zhibao Lv, Li Lu

zhibao1yu@163.com (Z.L.)
luli_2006@126.com (L.L.)

Highlights

HDAC8 was upregulated in NEC and suppressing HDAC8 could improve NEC

HDAC8 regulated the arginine-proline metabolism pathway during NEC development

H3K9ac was a substrate of HDAC8 to regulate the enzymes for arginine conversion

Butyrate inhibited HDAC8 expression and affected arginine concentration in NEC



Article

Elevated expression of histone deacetylase HDAC8 suppresses arginine-proline metabolism in necrotizing enterocolitis

Ting Guo,¹ Shaohua Hu,² Weijue Xu,¹ Jin Zhou,¹ Feng Chen,¹ Tingting Gao,¹ Wenqian Qu,¹ Faling Chen,¹ Zhibao Lv,^{1,*} and Li Lu^{1,3,*}

SUMMARY

Epigenetic alterations are especially important in necrotizing enterocolitis (NEC). Here, we reported that histone deacetylase 8 (HDAC8) plays a previously unknown role in modulating arginine metabolism via acetylation of histone 3 lysine 9 (acetyl-H3K9) regulation during the pathogenesis of NEC. We found that HDAC8 was upregulated in humans and mice intestinal samples with NEC, while selective inhibition of HDAC8 expression ameliorated NEC. HDAC8 regulates enzymes involved in the metabolic conversion of proline to arginine (PRODH, PRODH2, OAT, and OTC) and arginine to ornithine (ARG1). The results showed that H3K9ac signal in the PRODH/PRODH2 promoter region was mediated by HDAC8. Additionally, the decreased concentration of butyric acid was strongly correlated with elevated HDAC8 levels and circulating arginine, which may result from an unbalanced Firmicutes/Bacteroidetes ratio. These results reveal previously underappreciated roles of microbial metabolites and HDAC8 to coordinate the arginine metabolism during NEC development.

INTRODUCTION

Necrotizing enterocolitis (NEC) is one of the most common gastrointestinal emergencies in premature infants and is associated with a substantial mortality rate ranging from 15% to 30%.¹ Accumulated evidence suggests that NEC is a multifactorial and complex disease, which makes research on its pathogenesis difficult.

Arginine is an amino acid involved in several physiologic and metabolic pathways, including the host immune response, urea cycle, hormonal secretion, and nitric oxide production.^{2,3} The small intestine plays a major role in whole-body amino acid metabolism in neonates, and epithelial cells in the small intestine are the primary cells responsible for the synthesis of arginine (Arg) from glutamine (Gln), proline (Pro), and citrulline (Cit).^{4–6} According to previous study, infants who had NEC were found to have low circulating concentrations of amino acids, particularly Gln and Arg.^{7,8} Endothelial nitric oxide synthase (eNOS) converts L-arginine to endogenous nitric oxide (NO), and NO plays an essential role in NEC development by regulating vasodilatation and blood flow to the intestine.⁹ Gln was found to have beneficial effects on intestinal integrity and intestinal cell apoptosis by reducing TLR-2 and TLR-4 expression in the intestines of neonatal rats with NEC.^{10,11} Although amino acid supplementation was found to reduce the incidence of NEC and the mortality resulting from NEC,^{11,12} none of the studies focused on the mechanisms that cause these amino acid abnormalities that occur in NEC.

Premature birth, bacterial colonization, enteral feeding, and hypoxia are high-risk factors for NEC,¹³ and they likely to influence susceptibility to NEC through epigenetic mechanisms.¹⁴ The most well-known epigenetic changes are DNA methylation and post-translational modifications on histones.¹⁵ Emerging evidence indicates that DNA methylation contributes to changes in gene transcription and the establishment of signaling networks in NEC,^{16–18} but knowledge about histone modifications that occur in NEC is limited. Histone deacetylases (HDACs) are a family of enzymes that alter gene expression by deacetylating histones and are associated with multiple biological events,^{19,20} and the expression of HDACs is often perturbed in cancer, neurological syndromes, and immune disorders.²¹ HDACs are grouped into four classes: class I enzymes (HDAC1, 2, 3, and 8); class II enzymes (HDAC4, 5, 6, 7, 9, and 10); class III enzymes (SIRT1, 2, 3, 4, 5, 6,

¹Department of General Surgery, Shanghai Children's Hospital, School of Medicine, Shanghai Jiao Tong University, Shanghai 200040, China

²Department of Clinical Laboratory, Shanghai Children's Hospital, School of Medicine, Shanghai Jiao Tong University, Shanghai 200040, China

³Lead contact

*Correspondence:

zhibaoLv@163.com (Z.L.),

luli_2006@126.com (L.L.)

<https://doi.org/10.1016/j.isci.2023.106882>



Table 1. The criteria of patients

Patients' characteristics	Case (n=8)	Controls (n=8)	P value
Age at surgery	35.7	35.5	0.875
(weeks)	(31.1-39.7)	(31-39)	
Birth weight	1890	2250	0.093
(grams)	(1230-3280)	(1495-3415)	
Gender			0.522
Male	6(75%)	7(87.5%)	
Female	2(25%)	1(12.5%)	
Mode of birth			0.131
Spontaneous	3(37.5%)	2(25%)	
Caesarean	5(63.5%)	6(75%)	
Intraoperative diagnosis	NEC	congenital intestinal atresia and stenosis	
Sampling area	ileum	Ileum	

and 7); and class IV enzymes (HDAC11).²² An increasing number of studies have focused on the importance of short chain fatty acids (SCFAs) and have paid particular attention to the role of butyric acid in NEC,^{23,24} which usually acts as a weak HDAC inhibitor.²⁵ Given the importance of butyrate, we hypothesize that HDACs regulation is a central mechanism through which transcriptional changes occur in the intestine during the perinatal period in preterm newborns.

In the present study, we explored the exact role of HDACs in NEC and found that elevated HDAC8 concentration was an inducer of abnormal arginine metabolism during the pathogenesis of NEC. Butyric acid was found to be the only SCFA with a concentration that was altered in NEC, and its levels positively correlated with arginine levels. It was also a regulator of HDAC8. Interestingly, our results suggested that all these changes may be related to the composition of the microbial flora, especially the Firmicutes/Bacteroides ratio.

RESULTS

HDAC8 expression was upregulated in NEC

To investigate the potential role of HDACs in the pathogenesis of NEC, we first analyzed HDAC expression in neonatal intestinal tissues from humans and mice. The demographic and clinical characteristics of the NEC patients and control patients are shown in Table 1. The results demonstrated that HDAC4 and HDAC11 levels were lower in both humans and mice with NEC than in controls, but only HDAC8 levels were higher (Figure 1A). In this study, we mainly focused on the role of HDAC8, which belongs to the class I family in NEC. Western blotting and immunohistochemical staining (IHC) also revealed that HDAC8 protein expression was upregulated in NEC (Figures 1B and 1C). According to the IHC results, HDAC8 expression was found to be mainly localized in the intestinal epithelial cells (IECs) (Figure 1C). HDAC8 levels were observed to be increased in IECs isolated from the intestinal tissue of preterm humans and mice with NEC (Figure 1D), lipopolysaccharide (LPS)-treated FHs74Int cells, and LPS-treated IEC6 cells (Figure 1E). At the same time, we also isolated lamina propria lymphocytes (LPLs) from the intestinal tissue of preterm humans and mice with NEC, and there was no difference in HDAC8 expression in the LPLs between the controls and NEC (Figure 1F). In summary, these results illustrated that the expression of HDAC8 increased mainly in the IECs during the development of NEC.

Targeted inhibition of HDAC8 expression impedes the development of NEC

To determine whether HDAC8 promotes the development of NEC, we experimentally induced NEC in mice treated with a highly selective inhibitor of HDAC8 (PCI-34051),²⁶ and control mice to investigate whether HDAC8 expression inhibition could alleviate intestinal lesions in an NEC mouse model. The results showed that oral administration of PCI34051 effectively prevented intestinal NEC-like lesions, including thickening and pneumatosis (Figures 2A and 2B). Hematoxylin and eosin (H&E) staining of the terminal ileum and the histopathological scores demonstrated less severe changes in the NEC group subjected to HDAC8 expression inhibition than in the NEC group exhibiting normal HDAC8 expression

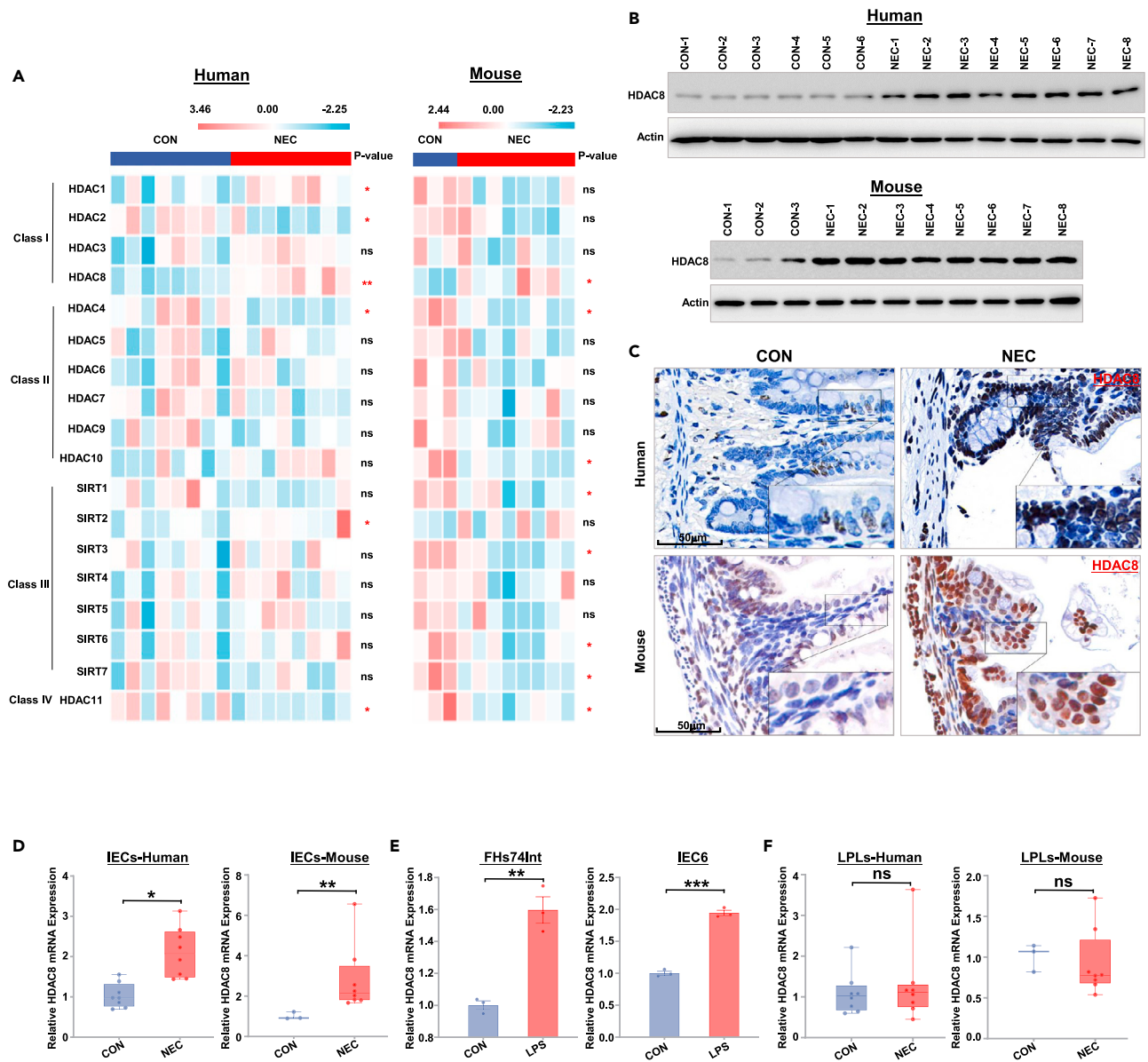


Figure 1. HDAC8 expression is upregulated in the intestine of humans and mice with NEC

(A) Heatmaps of HDAC expression in control and NEC samples (human: control = 8, NEC = 8; mice: control = 3, NEC = 8).

(B) HDAC8 protein levels were measured by Western blotting in healthy control and NEC samples.

(C) HDAC8 expression was assessed using immunostaining performed on the sections of the terminal ileum in healthy control and NEC samples. Scale bar: 50 µm.

(D) qRT-PCR was performed to assess the relative expression levels of HDAC8 in IECs isolated from humans and mice. *p < 0.05, **p < 0.01 (Mann-Whitney test).

(E) qRT-PCR was performed to assess the relative expression levels of HDAC8 in FHs74Int and IEC6 cells. **p < 0.01, and ***p < 0.001 (two-tailed Student's t test).

(F) qRT-PCR was performed to assess the relative expression levels of HDAC8 in LPLs isolated from humans and mice. ns means no significance (Mann-Whitney test).

(Figures 2C and 2D). Analysis of the villus height and crypt depth indicated that HDAC8 expression inhibition clearly reduced the severity of injury in mice with NEC (Figure 2E). We also evaluated inflammatory cytokine expression in the ileum. In the NEC groups, the expression levels of inflammatory cytokines, including IL-6, IL-1β, and TNF-α were noticeably increased. However, after HDAC8 expression inhibition,

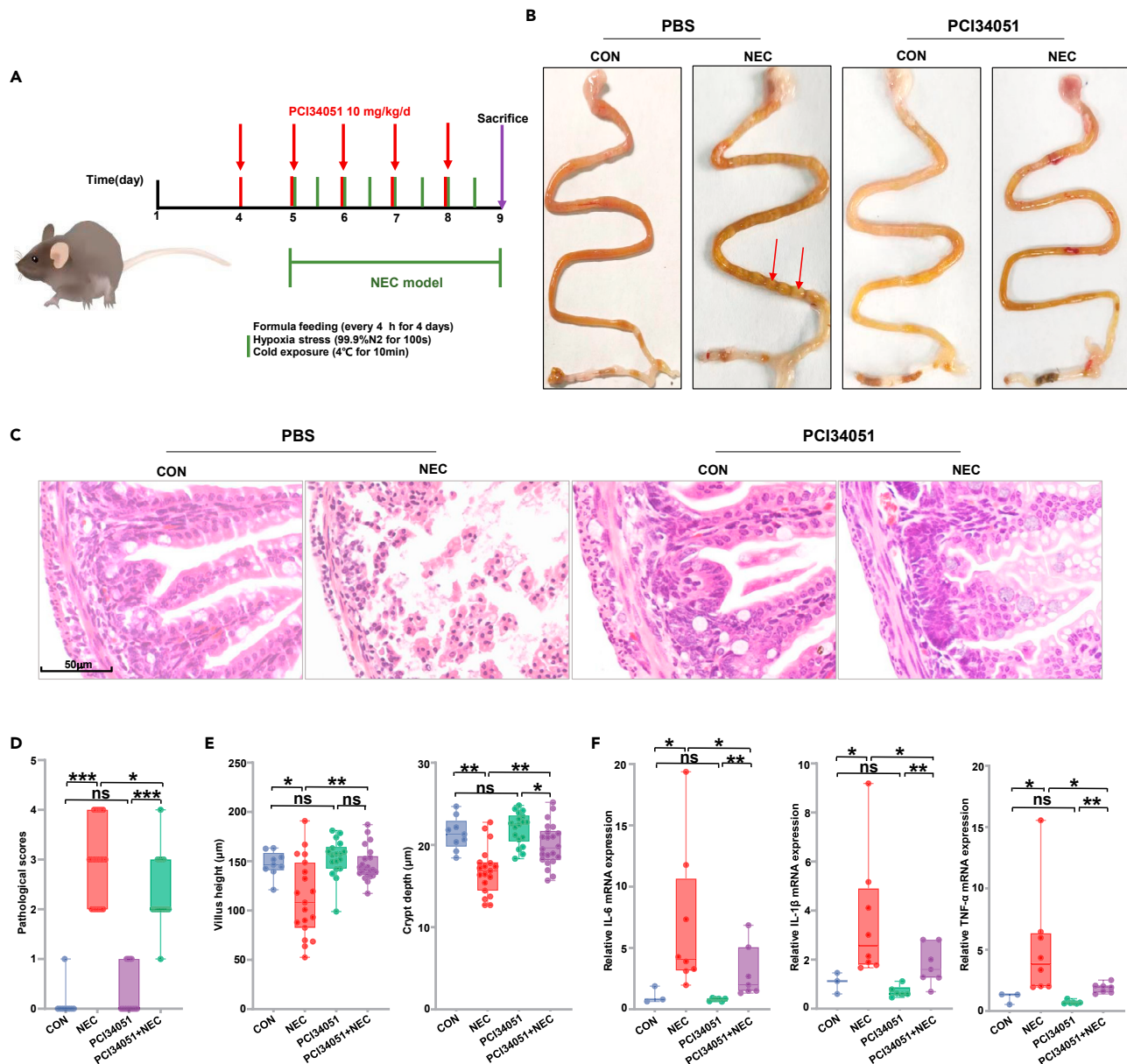


Figure 2. Selective HDAC8 inhibition ameliorates NEC

(A) Diagram of the experimental design using the mouse model.

(B) Representative images of intestinal samples from control mice and mice with NEC after PBS or PCI34051 treatment.

(C) Representative images of H&E staining of terminal ileum from control mice and mice with NEC treated with PBS or PCI34051. Scale bar: 50 μm.

(D) Histological scores denoting the severity of tissue lesions were determined in terminal ileum samples obtained from control mice (n = 9), mice with NEC (n = 19), PCI34051-treated mice (n = 18), and PCI34051-treated mice with NEC (n = 22). The pathological changes were scored as follows: Grade 0, normal ileum; Grade 1, injury of the villus tip; Grade 2, partial loss of villi; Grade 3, severe injury of the submucosa; and Grade 4, complete necrosis. Data were pooled from three independent experiments. The data in the boxplot are expressed as the means ± SEMs.

(E) Villus heights and crypt depths were measured and analyzed in samples from control and NEC mice treated with PBS or PCI34051. Data were pooled from three independent experiments. The data in the boxplot are expressed as the means ± SEMs.

(F) The mRNA expression levels of inflammatory factors, including IL-6, IL-1β, and TNF-α, in intestinal samples obtained from control mice (n = 3), mice with NEC (n = 8), PCI34051-treated mice (n = 6), and PCI34051-treated mice with NEC (n = 7). The data in the boxplot are expressed as the means ± SEMs. Three independent experiments were performed. *p < 0.05, **p < 0.01, ***p < 0.001. ns means no significance. Statistical significance was tested by Mann-Whitney test (D, E, F).

the levels of the indicated cytokines were decreased under the NEC modeling conditions (Figure 2F). These results further confirmed that HDAC8 was critical for the development of NEC.

HDAC8 regulates the arginine-proline metabolism pathway during the pathogenesis of NEC

To further explore the role of HDAC8 in NEC, we first analyzed the signaling pathways that were altered in humans and mice with NEC. Kyoto Encyclopedia of Genes and Genomes (KEGG) analysis revealed that the genes with altered expression in NEC were mainly enriched in metabolic and immune regulation-related pathways in the GSE46619 dataset containing human data (Figure 3A). The genes with downregulated expression were mainly involved in metabolism (Figure 3B), while the genes with upregulated expression were mainly involved in immune regulation (Figure 3C). There were 29 pathways enriched for by the differentially expressed genes in the NEC mouse model that coincided with those in humans (Figure 3D). The genes with downregulated expression were mainly involved in metabolism (Figure 3E), while the genes with upregulated expression were mainly involved in immune regulation (Figure 3F), which is consistent with the findings observed in NEC patients.

Next, we analyzed which signaling pathways may have been affected by HDAC8. Combining DESeq2 with Venn diagram analysis, we found that the expression of 2682 of 4054 downregulated genes in NEC were reversed after HDAC8 suppression, while the expression of 4045 of 4585 upregulated genes was decreased after HDAC8 suppression (Figure 4A and B). We considered these overlapping genes as genes regulated by HDAC8. The KEGG analysis of these genes indicated that HDAC8 maintained pathways including arginine and proline metabolism, mineral absorption, vitamin digestion, and absorption, peroxisome, metabolic pathways, *Staphylococcus aureus* infection, the MAPK signaling pathway, and the PI3K-Akt signaling pathway during the development of NEC (Figure 4C). We next used a Rank-Rank Hypergeometric Overlap (RRHO) analysis to confirm the results. RRHO analysis indicated a substantial overlap of the genes regulated by HDAC8 (Figure 4D), and the result showed that 15420 downregulated genes were reversed and 223 upregulated genes were repressed after HDAC8 expression inhibition (Figure 4E). We conducted KEGG analysis of these overlapping genes and the results were similar with those obtained with DESeq2 analysis, especially arginine and proline metabolism, mineral absorption, vitamin digestion, and absorption, peroxisome, the MAPK signaling pathway, and the PI3K-Akt signaling pathway (Figure 4F). Considering the importance of arginine metabolism in NEC, we decided to focus our follow-up study on the mechanism by which epithelial HDAC8 regulates arginine metabolism.

HDAC8 maintains arginine metabolism by regulating the expression of metabolic enzymes in NEC

We next measured the ileum concentrations of amino acids in mice with NEC. The results showed that the concentrations of Arg, tyrosine (Tyr) and leucine (Leu) were significantly lower in the mice with NEC than in the controls. In contrast, phenylalanine (Phe) levels were significantly increased. However, inhibition of HDAC8 expression only reversed the changes in the concentration of arginine (Figure 5A). To reveal the mechanism, we measured the expression of arginine metabolic enzymes, and the results showed that the expression of the arginine synthesis enzymes PRODH, PRODH2, ALDH18A1, OAT, OTC, ASS1, ASL, and CPS1 were significantly lower in IECs isolated from mice with NEC than in the controls, while the decreases in PRODH, PRODH2, OTC, and OAT levels were reversed in the HDAC8 expression inhibited group (Figure 5B). In addition, the catabolic enzymes GATM and NOS1 exhibited downregulated expression in IECs isolated from mice with NEC, while no difference in NOS2 or NOS3 expression was observed between the controls and mice with NEC. Although ARG1 and ARG2 levels were increased in NEC tissues, only ARG1 expression was suppressed under conditions of HDAC8 expression inhibition (Figure 5C). Moreover, further research showed that the effect on the five enzymes could be reversed by HDAC8 in FHs74Int cells (Figure 5D). As summarized in Figure 5E, these results suggested that arginine synthesis in NEC was diminished by decreases in the synthesis of ornithine from glutamine and proline through ALDH18A, PRODH/PRODH2 and OAT; the conversion of ornithine to citrulline through CPS1 and OTC; and the recycling of citrulline to arginine by ASS1 and ASL. However, robust arginine catabolism was induced by an increase in the conversion of arginine to ornithine through ARG1 and AGR2. In summary, our results showed that among all arginine metabolic pathways, only the synthesis of ornithine from proline through PRODH, PRODH2, and OAT; the conversion of ornithine to citrulline through OTC; and the conversion of arginine to ornithine through ARG1 were regulated by HDAC8.

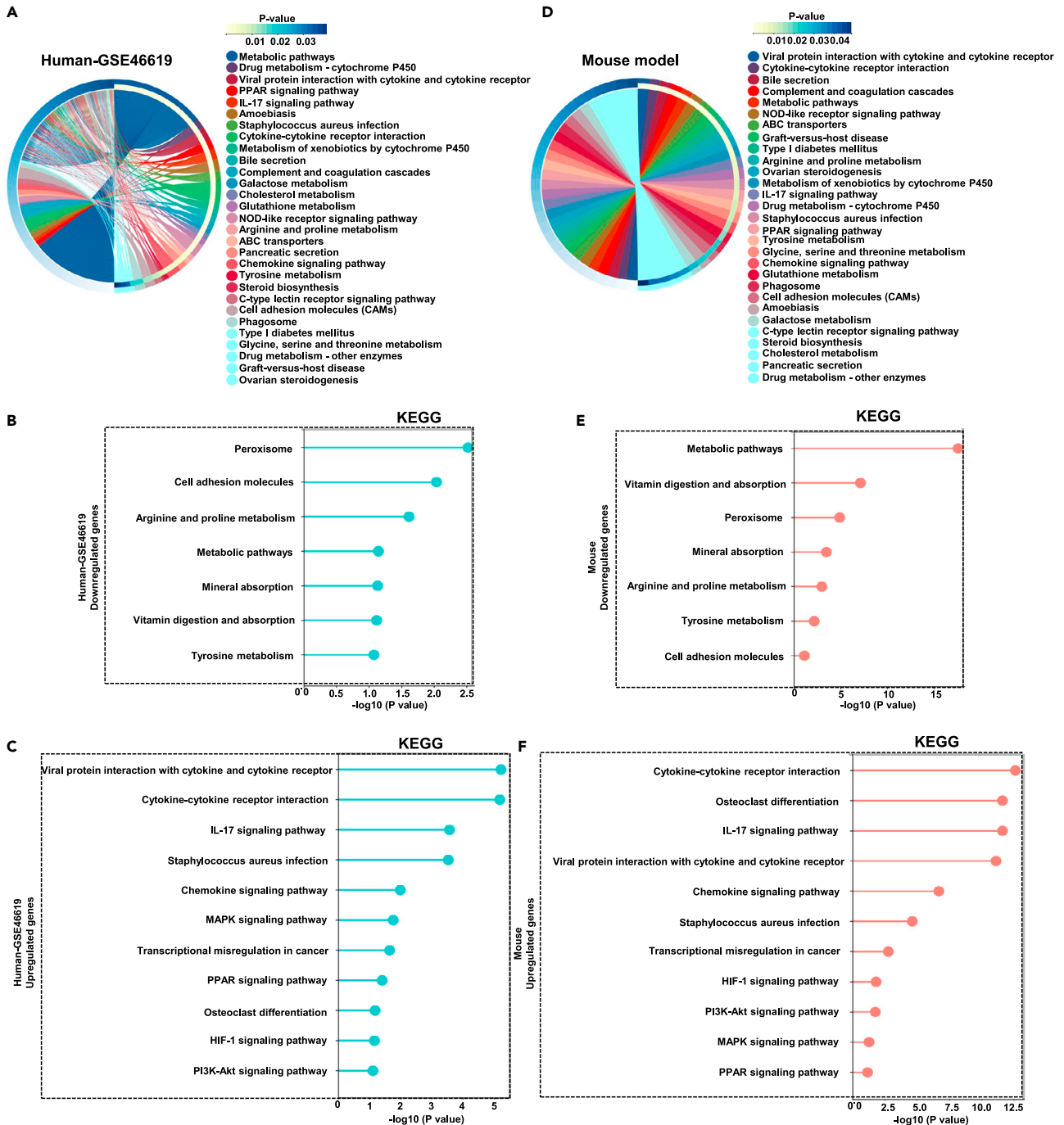


Figure 3. Altered pathways in NEC

(A) KEGG pathways significantly enriched for by the differentially expressed genes between NEC and control samples from preterm infants from the GSE46619 dataset. The selection criteria for differentially expressed genes were $|\text{Log}_2\text{FC}| > 1$ and $p < 0.05$.

(B and C) KEGG pathways significantly enriched for by the downregulated (B) and upregulated (C) genes in humans.

(D) KEGG pathways significantly enriched for by the differentially expressed genes between NEC and control samples in the mouse model. The selection criteria for differentially expressed genes were $|\text{Log}_2\text{FC}| > 1$ and $p < 0.05$.

(E and F) KEGG pathways significantly enriched for by the downregulated (E) and upregulated (F) genes in mice.

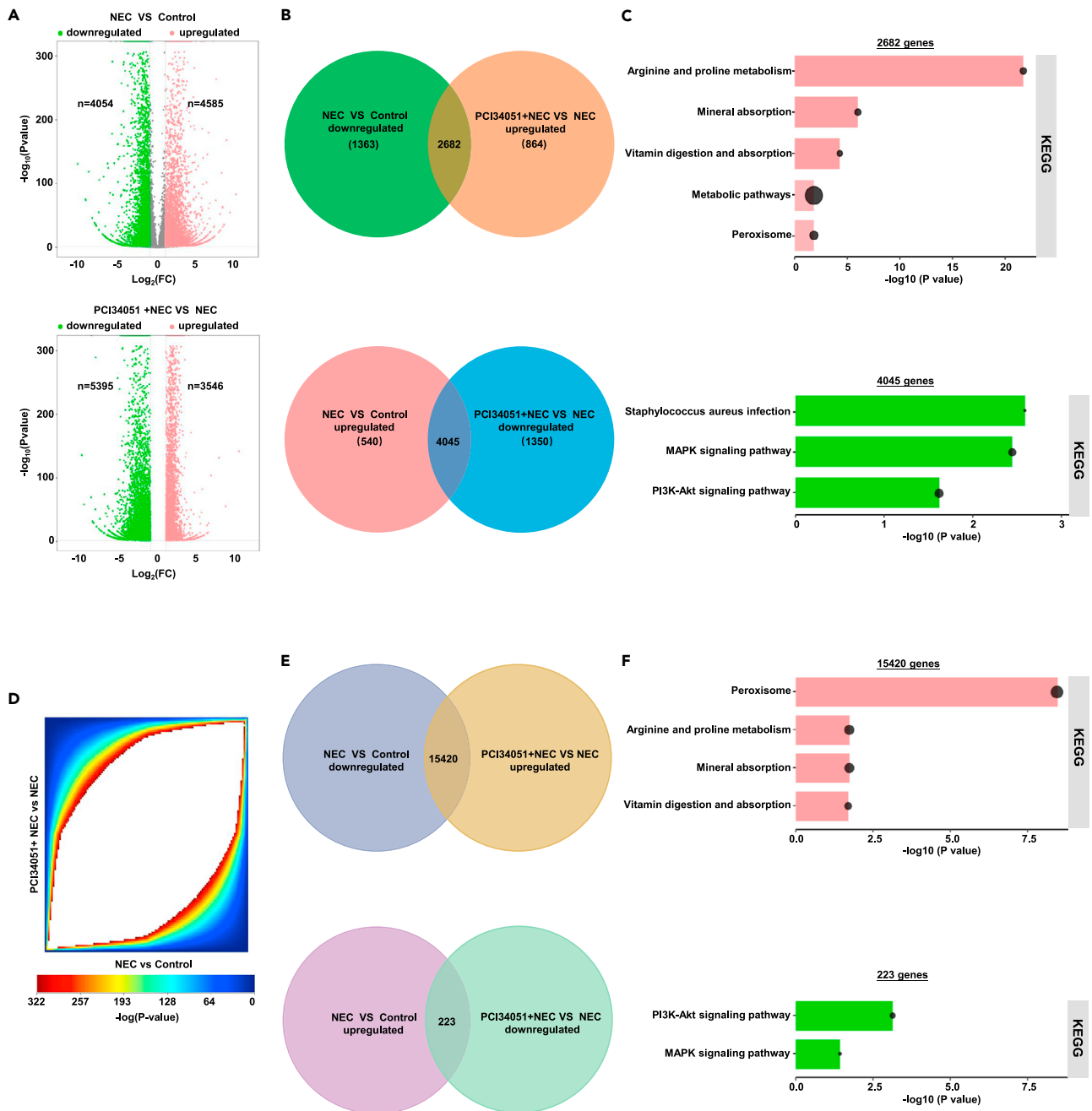


Figure 4. Analysis of pathways regulated by HDAC8 in NEC

(A) Volcano plots were generated to infer the overall distribution of differentially expressed genes between NEC and control groups (upper panel); volcano plot shows the differentially expressed genes after PCI34051 treatment in the NEC group (lower panel). Genes were analyzed by DEseq2 and identified based on the cut off criterion: p values < 0.05 , and $|\log_2fc| > 1$.

(B) Venn diagrams showing the overlapping genes with genes downregulated in NEC and genes upregulated after PCI34051 treatment (upper panel); Venn diagrams showing the overlapping genes with genes upregulated in NEC and genes downregulated after PCI34051 treatment (lower panel).

(C) KEGG pathway enrichment results for the genes regulated by HDAC8 in NEC.

(D) RRHO maps comparing NEC vs. control group and PCI34051+ NEC vs. NEC group. Degree of significance is depicted in the color bar below the RRHO maps.

(E) Venn diagram displaying the overlap between genes downregulated in NEC and upregulated after PCI34051 treatment (upper panel); Venn diagram displaying the overlap between genes upregulated in NEC and downregulated after PCI34051 treatment (lower panel). The overlapping genes were obtained from RRHO analysis.

(F) Pathway enrichment analysis for the [Figure 4E](#) overlapping genes, which are similar with the results analyzed by DEseq2.

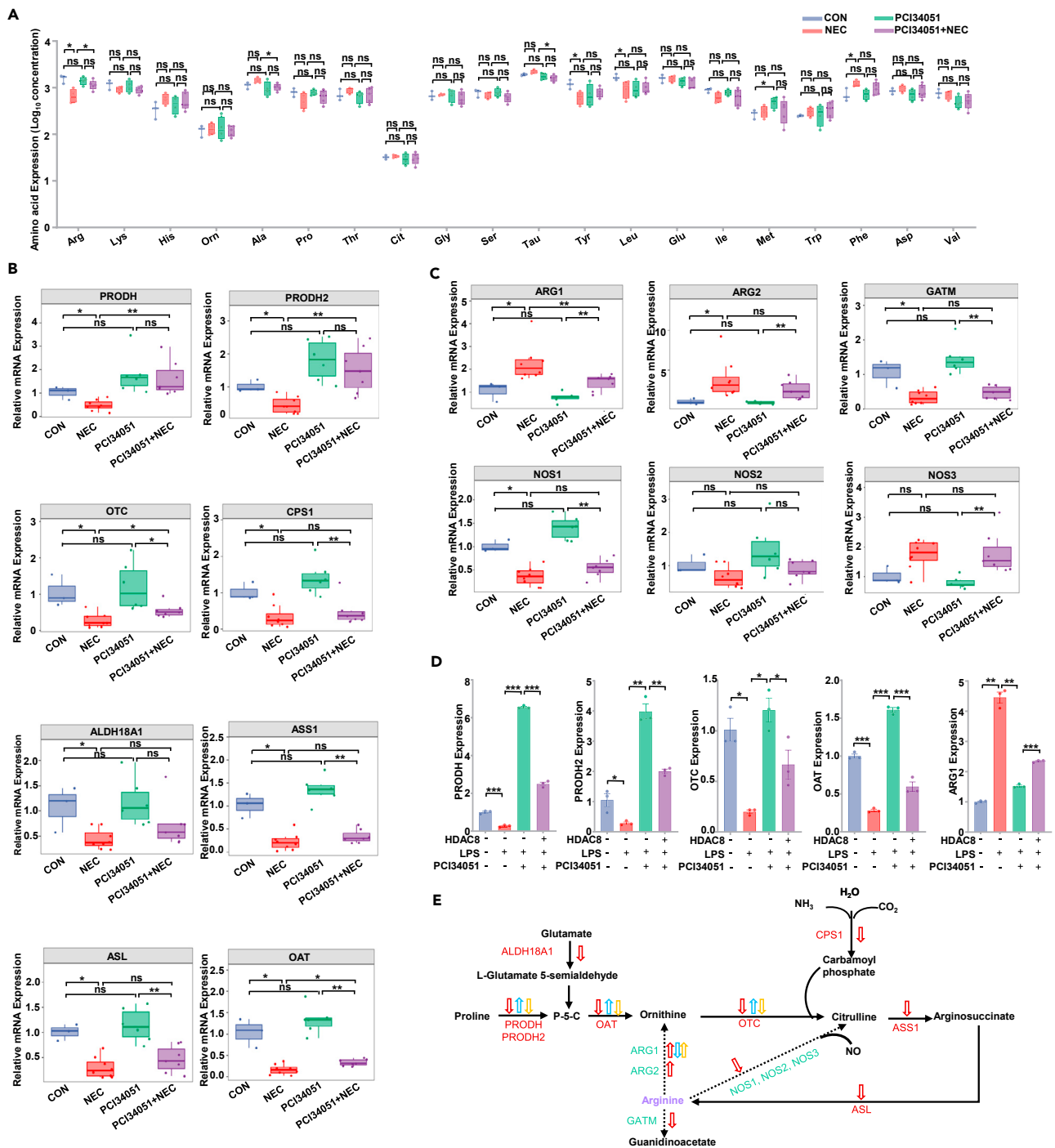


Figure 5. HDAC8 regulates the expression of amino acid metabolic enzymes in NEC

(A) Analysis of intestinal amino acid concentrations ($\mu\text{g/g}$) in mice in the control group ($n = 3$), NEC group ($n = 4$), PCI34051 group ($n = 4$), and PCI34051+ NEC group ($n = 5$).

(B and C) qRT-PCR analysis was performed to assess the relative expression level of enzymes known to be required for arginine synthesis (B) and arginine catabolic process (C) in IECs isolated from intestinal samples obtained from control mice ($n = 3$), mice with NEC ($n = 8$), PCI34051-treated mice ($n = 6$) and PCI34051-treated mice with NEC ($n = 7$). The results are expressed as the means \pm SEMs. Three independent experiments were performed.

Figure 5. Continued

(D) The levels of enzymes regulated by PCI34051 in the intestine were compared in the indicated groups of FHs74Int cells. The results are expressed as the means \pm SEMs. Three independent experiments were performed.

(E) Schematic representation of the changes in arginine metabolic enzymes in response to inflammatory conditions (red arrows), PCI34051 treatment (blue arrows), and HDAC8 overexpression (yellow arrows). * $p < 0.05$, ** $p < 0.01$, *** $p < 0.001$. ns means no significance. Statistical significance was tested by Mann–Whitney test (A, B, C) or two-tailed one-way analysis of variance test (D).

H3K9ac is a potential substrate of HDAC8 that regulates the expression of arginine-proline metabolic enzymes

To identify the downstream mechanisms by which HDAC8 regulates the expression of arginine metabolic enzymes in NEC, we quantified the changes in the levels of H3K9ac, H3K14ac, H3K27ac, and H4K16ac, which have been recognized as substrates of HDAC8. Among these four histone acetylation sites, only the acetylation of H3K9 was found to exhibit a decreased level in intestinal tissues in NEC (Figure 6A), and the decrease in acetyl-H3K9 levels was reversed when HDAC8 expression was inhibited (Figure 6B). In FHs74Int and IEC6 cells, LPS induced a significant increase in HDAC8 expression along with the deacetylation of H3K9, and PCI34051 treatment suppressed the increase in HDAC8 expression and subsequent deacetylation of H3K9. However, the acetylation level of H3K9 decreased significantly in HDAC8-overexpressing cell lines (Figure 6C). To verify that arginine metabolic enzymes are directly regulated by H3K9ac, we performed a CUT&Tag assay to assess the changes in the H3K9ac signals at these genes. The results suggested a decrease in the H3K9ac signal in the PRODH and PRODH2 promoters upon LPS stimulation, while HDAC8 inhibition elevated the acetyl-H3K9 signal around the PRODH and PRODH2 promoter regions. Moreover, there was a decrease in the acetyl-H3K9 level in the PRODH and PRODH2 promoters in HDAC8-overexpressing cells (Figure 6D). Consistently, the chromatin immunoprecipitation (ChIP) assay also revealed that PCI34051 increased the binding of H3K9ac to the PRODH and PRODH2 promoters, while ectopic expression of HDAC8 decreased the levels of acetyl-H3K9 around the PRODH and PRODH2 promoters (Figure 6E). Therefore, we proposed that the HDAC8-mediated H3K9ac signal in the PRODH/PRODH2 promoter region inhibits their expression in IECs in NEC.

Decreased butyrate concentration is correlated with the arginine concentration in NEC

Next, we considered the reasons for the increase in HDAC8 levels that is observed clinically. We first considered that the metabolites of the intestinal flora may be related to this finding. Ultra-high performance liquid chromatography-mass spectrometry (UPLC–MS/MS) was used to measure the concentrations of SCFAs in 13 NEC and 13 paired control samples. As shown in Table 2, 26 preterm infants were enrolled in the study. The controls were well matched to the NEC patients in terms of clinical factors, and there was no statistically significant difference in gestational age, sex, birth weight, mode of delivery, or sampling time between the infants with NEC and the control infants. Moreover, all enrolled infants were fed preterm formula milk or human donor milk, and the difference in the ratio of the use of different milk types was not significantly different between the two groups. In addition, the difference in the Apgar score, which is used to assess neonatal asphyxia, was not statistically significant. Only the positive fecal occult blood test rate differed between the NEC patients and the controls. The results of SCFA analysis revealed significantly different concentrations of butyric acid, but no significant differences between the two groups were identified in the levels of acetic acid, propionic acid, isobutyric acid, valeric acid, isovaleric acid, caproic acid, isocaproic acid, or lactic acid (Figure 7A). We also measured the concentrations of amino acids in plasma obtained from children with NEC. The results showed that the concentrations of arginine, proline, leucine, isoleucine, and valine were significantly lower in the children with NEC than in the controls (Figure 7B). Moreover, correlation analysis indicated that butyrate concentration was positively correlated with arginine concentration (Figure 7C).

In addition to revealing the reason for the decreased butyric acid concentration, we analyzed the gut microbiota composition, which might directly or indirectly influence SCFA concentrations. The composition of the microbiota was analyzed by 16S rRNA sequencing. Pearson correlation analysis was used to establish the relationship between abundant bacteria at the phylum and class levels. The results suggested that the abundance of Firmicutes (especially Clostridia) exhibited moderate positive correlations with the butyric acid concentration (Figure 7D), while the abundance of Bacteroidetes (especially Bacteroidia) was moderately negatively correlated with the butyric acid concentration (Figure 7E). However, there was no correlation between the abundances of Proteobacteria (especially Gammaproteobacteria) (Figure 7F) and Actinobacteria (Figure 7G) and the butyric acid concentration. Interestingly, we observed a strong

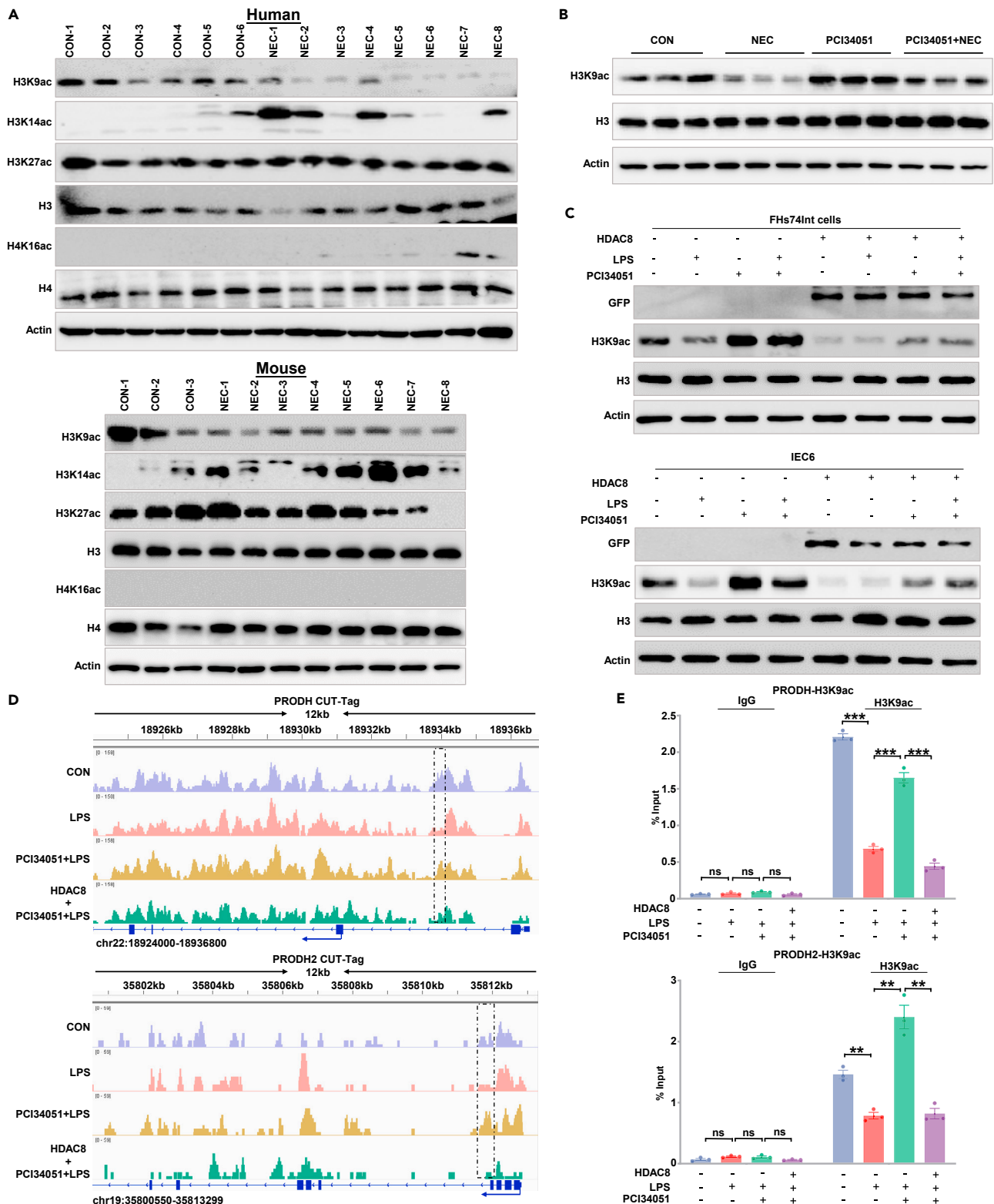


Figure 6. HDAC8 maintains arginine metabolism enzymes by regulating H3K9ac activity

(A) Western blotting analysis was performed to assess the relative expression levels of genes known to be substrates of HDAC8 in healthy controls and NEC samples obtained from humans (upper panel) and mice (lower panel).

Figure 6. Continued

(B) Western blotting analysis was performed to assess the relative expression levels of genes known to be substrates of HDAC8 in IECs isolated from mice. Three independent experiments were performed.

(C) The protein levels of HDAC8, H3K9ac, H3K14ac, H3K27ac, and H4K16ac were analyzed by Western blotting in FHs74Int and IEC6 cells transfected with control lentivirus and HDAC8 lentivirus with 10 μmol/L PCI34051 incubation for 24 h and 10 μg/mL LPS for 48 h.

(D) H3K9ac-binding profiles on the targeted gene promoter detected by CUT-Tag in FHs74Int cells.

(E) ChIP analysis of H3K9ac in the PRODH and PRODH2 promoters under the conditions of PCI34051 (10 μmol/L for 24 h) or LPS (10 μg/mL for 48 h) treatment in control or HDAC8 stably overexpressing FHs74Int cells. The results are expressed as the means ± SEMs. Three independent experiments were performed. **p < 0.01, ***p < 0.001. ns means no significance. Statistical significance was tested by two-tailed one-way analysis of variance test (E).

positive correlation ($R = 0.82$, $p = 3.4e-07$) between the Firmicutes/Bacteroidetes ratio and the butyric acid concentration (Figure 7H). These results revealed that the Firmicutes/Bacteroidetes ratio is an important indicator of dysbiosis and may be associated with the altered concentration of butyric acid in NEC. All these results suggested that the decreased butyrate concentration may be caused by the change in the relative Firmicutes/Bacteroidetes ratio, and butyrate concentration is positively correlated with the concentration of arginine in the clinic.

Butyrate selectively inhibits epithelial HDAC8 expression during the pathological progression of NEC

We next detected whether HDAC8 can affect by the production of butyrate. The mRNA expression analysis showed significant decreases in the levels of the histone deacetylases HDAC1, HDAC4, HDAC6, HDAC10, SIRT1, SIRT3, SIRT6, and SIRT7 in NEC tissues, but their levels were not affected by butyrate. Only the level of HDAC8 was found to be significantly increased in NEC and reduced by butyrate (Figure 8A). Consistent with this finding, butyrate declined HDAC8 expression in IECs isolated from the intestinal tissue of mice (Figure 8B) and in FHs74Int cells and IEC6 cells (Figure 8C). The protein level of HDAC8 as determined by IHC and Western blotting analysis suggested the same regulatory trend as that observed in the mRNA level (Figures 8D and 8E). Among the four histone acetylation sites, only the H3K9ac signal was

Table 2. General situation of control and case group

Factors	CON (n=13)	NEC (n=13)	χ^2	P value
Gestational age (weeks of completed gestation)	29.9 (27.3-31.4)	29.7 (26-34.7)		0.472
Birth weight (grams)	1393.8 (870-1760)	1290 (1000-1800)		0.209
Gender			0 ^a	1
Male	9 (69.2%)	9 (69.2%)		
Female	4 (30.8%)	4 (30.8%)		
Mode of birth			1.385 ^a	0.239
Spontaneous	5 (38.5%)	8 (61.5%)		
Caesarean	8 (61.5%)	5 (38.5%)		
Sampling time (days of gathering the sample after birth)	14.7 (2-33)	31.8 (4-101)		0.28
Enteral feeds			1.188 ^a	0.552
Donor milk	7 (53.8%)	6 (46.2%)		
Formula milk	1 (7.7%)	3 (23.1%)		
Compound	5 (38.5%)	4 (30.7%)		
Apgar scores				
1 min	7.4 (4-8)	7.4 (5-9)		0.881
5min	8.5 (7-9)	8.4 (6-10)		0.927
Fecal occult blood			19.067 ^a	< 0.001
Positive	2 (15.4%)	13 (100%)		
Negative	11 (84.6%)	0 (0%)		

^a0 cells (.0%) have expected count less than 5.

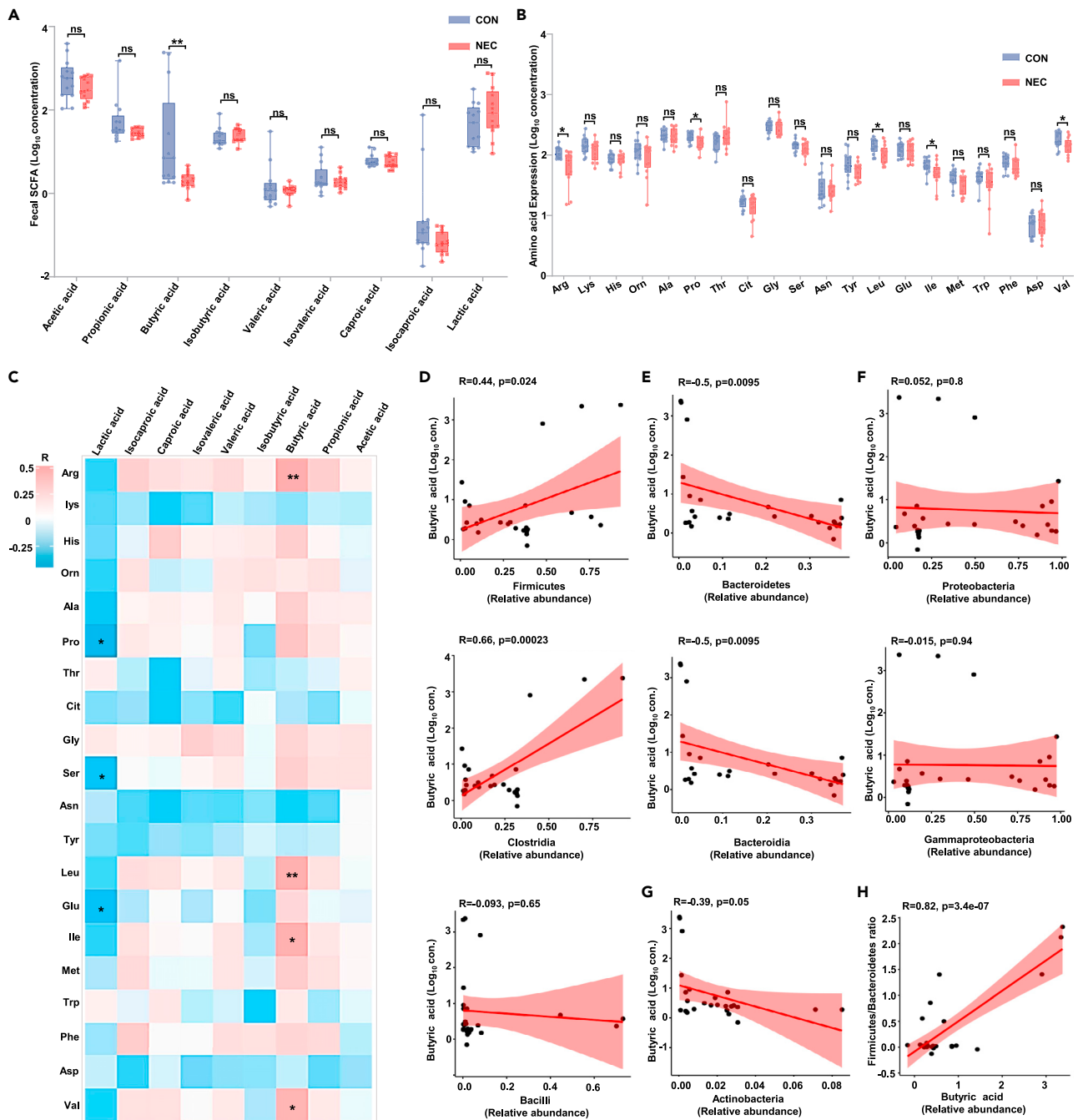


Figure 7. Butyrate concentration is positively correlated with arginine concentration in the clinic

(A) The log₁₀ of SCFA concentration (nmol/g). Analysis of SCFA concentrations in fecal samples from NEC patients (n = 13) and controls (n = 13).

(B) Analysis of serum amino acid concentrations in NEC patients (n = 13) and controls (n = 13).

(C) Correlations between the concentrations of SCFAs and amino acids.

(D–G) Correlations between the concentration of butyric acid and abundances of dominant bacteria, including Firmicutes, Clostridia and Bacilli (D); Bacteroidetes and Bacteroidia (E); Proteobacteria and Gammaproteobacteria (F); and Actinobacteria (G). Pearson correlation coefficients (R) and p values (p) are denoted. The lines represent the linear regression lines.

(H) Correlations between the concentrations of butyric acid and the Firmicutes/Bacteroidetes ratios. Pearson correlation coefficients (R) and p values (p) are denoted. The line represents the linear regression line. *p < 0.05, **p < 0.01. ns means no significance. Statistical significance was tested by Mann–Whitney test (A, B).

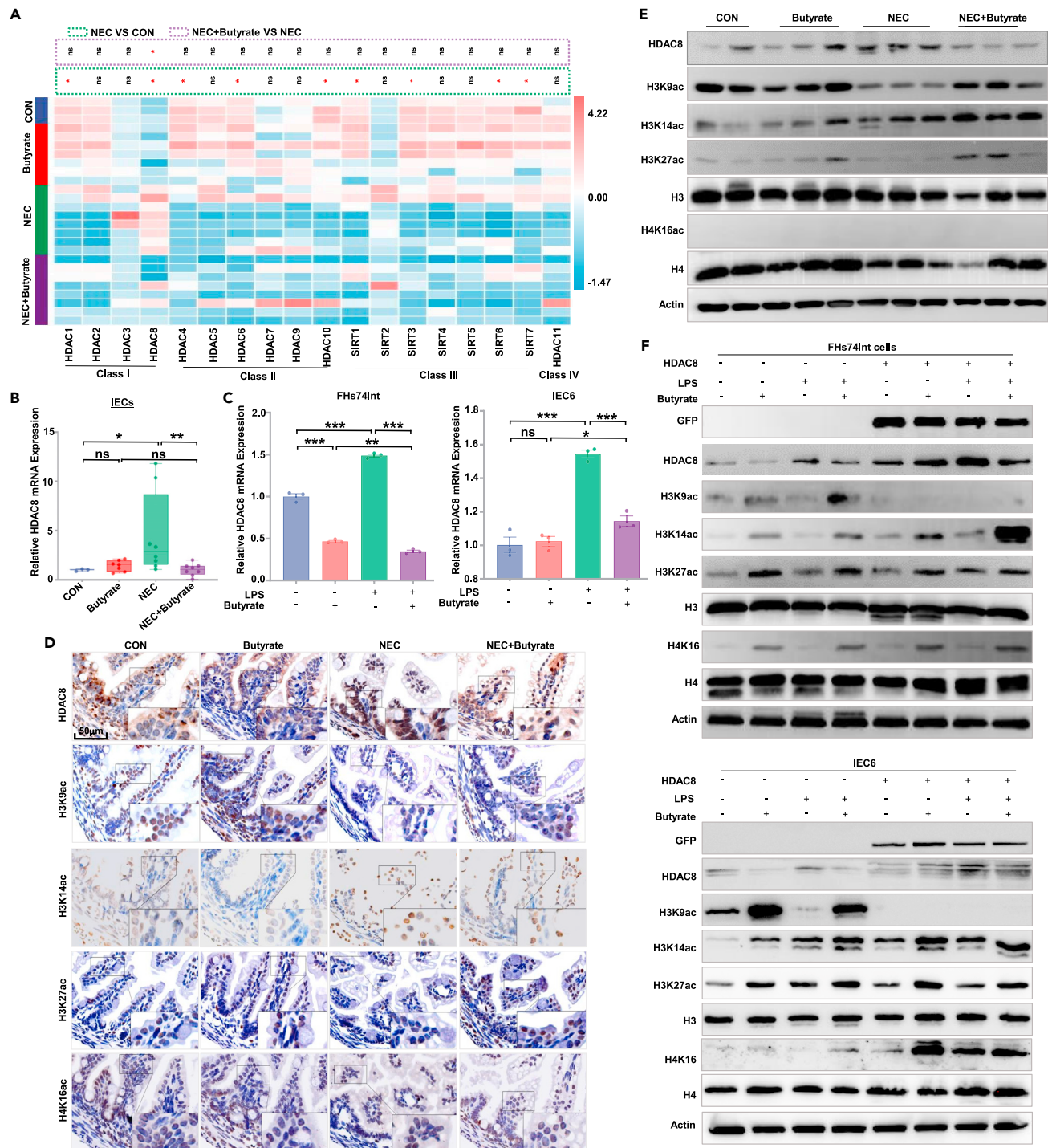


Figure 8. Butyrate inhibits HDAC8 in IECs

(A) qRT-PCR analysis of HDAC expression levels in terminal ileum samples obtained from the control mice (n = 3), butyrate-treated mice (n = 7), mice with NEC (n = 8), and butyrate-treated mice with NEC (n = 8). The data are shown in a heatmap. Three independent experiments were performed.

(B) Analysis of HDAC8 mRNA levels in IECs isolated from intestinal samples from control mice (n = 3), butyrate-treated mice (n = 7), mice with NEC (n = 8), and butyrate-treated mice with NEC (n = 8). Three independent experiments were performed.

(C) FHs74Int and IEC6 cells were incubated with LPS (10 µg/mL, 48 h) or butyrate (2 mmol/L, 12 h) as indicated. HDAC8 mRNA levels were analyzed by qRT-PCR. The results are expressed as the means ± SEMs. Three independent experiments were performed.

Figure 8. Continued

(D) IHC detection of HDAC8 expression and the expression of molecules known to be substrates of HDAC8 in terminal ileum samples obtained from the different groups as indicated. Scale bar: 50 μ m.

(E) Western blotting analysis was performed to assess the relative expression levels of HDAC8 and genes known to be substrates of HDAC8 in IECs isolated from the different groups as indicated.

(F) The protein levels of HDAC8, H3K9ac, H3K14ac, H3K27ac, and H4K16ac were analyzed by Western blotting in FHS74Int and IEC6 cells transfected with control lentivirus and HDAC8 lentivirus with 10 μ g/mL LPS for 48 h and 2 mmol/L butyrate stimulation for 12 h as indicated. * $p < 0.05$, ** $p < 0.01$, *** $p < 0.001$. ns means no significance. Statistical significance was tested by two-tailed one-way analysis of variance test (A, B) or Mann-Whitney test (C).

found to be reversed after butyrate supplementation (Figure 8D). This result was also observed in IECs (Figure 8E). In FHS74Int and IEC6 cells, LPS induced a significant increase in HDAC8 expression along with the deacetylation of H3K9, and butyrate treatment suppressed the increase in HDAC8 expression and subsequent deacetylation of H3K9 (Figure 8F). Collectively, these results suggest that butyrate selectively suppresses epithelial HDAC8 expression and its target during the pathological progression of NEC.

DISCUSSION

Even after decades of research, the specific pathogenesis of NEC remains unclear. Here, we analyzed the expression of histone deacetylase in NEC for the first time. We found that levels of HDAC8, which belongs to the class I family, were increased in the intestines in both humans and mice with NEC, and the selective inhibition of HDAC8 expression protected mice from NEC. Substantial progress in the development of HDAC inhibitors has been made in murine models and clinical trials for tumor treatment,²⁴ which also brings new hope for the future of the treatment of NEC.

In addition, our study revealed the reason for the upregulation of HDAC8 expression in NEC from the perspective of the microbial flora and its metabolites. The ability of butyrate to influence the function of IECs is related to its regulatory effects on gene, which are often thought to be involved in the inhibition of HDAC activity.²⁷ In our study, butyrate was found to suppress the expression of HDAC8 in mouse model, but the mechanism didn't be further explored in our study. We believe that identifying the relationship between butyrate and HDAC8 expression using a better cohort and exploring the regulatory mechanism is a good research direction in the future. Otherwise, our data showed that butyrate had no statistically significant effect on the expression of HDACs in the immature intestine under normal conditions but suppressed HDAC8 expression under inflammatory conditions. This finding is somewhat inconsistent with the previously reported findings observed in the mature intestine,^{27,28} perhaps due to the existence of different regulatory mechanisms in the immature intestine. In addition to HDAC8, we identified several other histone deacetylases with abnormal expression in NEC. Based on our previous findings that epigenetic reprogramming factors, including genes encoding histone H3K27 demethylation-associated proteins, enhancer binding proteins, and histone deacetylases, are methylated in NEC,²⁹ we believe that the regulation of histone modification plays a very important role in the occurrence and development of NEC. Previous studies have suggested that SCFAs alter chemokine expression in the epithelium and enhance the recruitment of neutrophils and lymphocytes into the intestine.^{30,31} Moreover, the contents of SCFAs varied with the establishment of flora, but no studies have established a clear relationship between butyric acid and the microbiota in NEC. The human gut microbiota mostly comprises two dominant bacterial phyla, Firmicutes and Bacteroidetes, which constitute more than 90% of the total community, and other subdominant phyla, including Proteobacteria, Actinobacteria, and Verrucomicrobia.³² Dysbiosis in NEC was found to be characterized by an increased relative abundance of Proteobacteria and decreased relative abundances of Firmicutes and Bacteroidetes in a meta-analysis.³³ However, some studies found that the microbial profile in NEC was dependent on the age at disease onset. Early onset NEC was associated with a dominance of Firmicutes, and late-onset NEC was associated with a decrease in Firmicutes abundance and an increase in Gammaproteobacteria abundance.^{34–37} We tried to establish a correlation between butyric acid and a single bacterium, but the results were not ideal, and there was an obvious strong correlation between the butyric acid concentration and the Firmicutes/Bacteroidetes ratio, which also suggests that the Firmicutes/Bacteroidetes ratio may be an important indicator of floral abnormalities in NEC. Moreover, it has been proposed that Firmicutes are more effective in extracting energy from food than Bacteroidetes, thus promoting more efficient absorption of calories and subsequent weight gain,³⁸ and this phenomenon may also be the reason for the limited weight gain observed in sick children with NEC. However, due to the small number of samples, we did not observe a good correlation between the abundances of different members of the flora and butyric acid concentration at other phylogenetic levels (data not shown).

In the small intestine, arginine can be synthesized from the precursors glutamine, proline, and citrulline.³⁹ Our results are consistent with previous reports that in NEC, the expression of arginine synthesis enzymes distributed in all pathways is generally decreased, while that of the arginases ARG1 and ARG2 are increased.⁸ This result demonstrated that the overall reduction in arginine synthesis and increased conversion of arginine to ornithine could lead to a reduced arginine concentration, which further confirmed our result that the arginine concentration was significantly decreased in the serum of preterm infants with NEC. We also observed that neither of the ornithine and citrulline are statistically significant decreased in NEC in the current cohort. Our qRT-PCR studies demonstrated that mRNA expression of OTC, OAT, CPS1, ASS1, NOS1, and NOS2 declined, but mRNA expression of ARG1, ARG2, and NOS3 augmented in NEC. Importantly, metabolism of these enzymes may offset one another, which may be the reason for the insignificant decrease of two amino acids. Given that the activity of amino acid metabolic enzymes usually matched enzymes expression levels,^{40–42} it is worthy to further confirm the changes in gene expression and activity level of these enzymes.

Among the involved pathways, the metabolism of proline and arginine (via PRODH, PRODH2, OAT, and OTC), and the conversion of arginine to ornithine (via ARG1) were found to be the primary pathways regulated by HDAC8. Moreover, acetylation of H3K9 regulated by HDAC8 has a regulatory relationship only with the promoter region of PRODH and PRODH2, which constitutes the first regulatory mechanism of arginine metabolic enzymes in infants with NEC and suggests that there are other mechanisms underlying the regulation of OTC, OAT, and ARG1 by HDAC8. This reasoning is also based on the fact that HDAC8 recognizes a large pool of acetylated nonhistone proteins as substrates.¹⁹ Additionally, there are two types of genes expressed in IECs. In addition to the genes encoding the proteins necessary for the functions of the cells as described above, another type of gene acts as a signal between epithelial cells and the mucosal immune system.

Microbial butyric acid has been proven to be a regulator of Tregs in NEC,²⁴ but the regulatory mechanism is unknown. Our unpublished data suggested that HDAC8 could influence IECs to produce inflammatory factors. Our findings prompted us to speculate that these inflammatory factors could enter the intestinal microenvironment and participate in the regulation of T cell differentiation, which will be the key focus of our future research.

In this study, we found that several SCFAs had a decreasing trend, but only butyric acid exhibited a significant decrease in NEC, and it was related to the development of the disease. The result indicating the change in butyric acid in NEC patients is supported by another study,²⁴ we speculated that butyric acid concentration is associated with the progression of disease, and we will further analyze the relationship between the butyric acid concentration and the progression of NEC. Of course, another important factor affecting this result is that the preterm babies were fed donated breast milk. Based on the current research, we can at least suggest that butyrate supplementation is an optional strategy for conservative NEC treatment.

In conclusion, we believe that the most important finding in this study was our determination of the regulatory role of HDAC8 in preterm infants with NEC. The histone deacetylase HDAC8 is an epigenetic-modifying enzyme that links butyric acid to intestinal epithelial arginine-proline metabolism maintenance.

Limitations of the study

In vitro and *in vivo* models, this study demonstrated that the epigenetic effector molecule HDAC8 regulates intestinal epithelial arginine-proline metabolism during the pathological progression of NEC. However, the study has potential limitations. HDAC8-inhibited (PCI-34051-treated) mice, which simulated HDAC8 knockout mice, are used in this study to prove that arginine metabolism indeed depends on HDAC8 expression inhibition and positively affects the outcome of NEC. In the following research, we will use HDAC8 knockout mice to further explore the mechanism. In addition, we demonstrated that the concentration of butyric acid may be caused by an unbalanced Firmicutes/Bacteroidetes ratio. We will collect more samples, and next correlate the concentration of butyric acid and the Firmicutes/Bacteroidetes ratio with the progression of disease to verify the direct link between the Firmicutes/Bacteroidetes ratio and butyric acid. These studies would further complement and establish the Firmicutes/Bacteroidetes ratio may have significant potential as a biomarker with respect to the diagnostic/predictive detection of NEC. Meanwhile, we couldn't establish a correlation between butyric acid

and bacterium at class and genus level. We realize that our results are limited to those obtainable with the detection and analysis methods used. Introducing new detection and analysis methods into our study may be more helpful in establishing the exact relationship between butyric acid and the microbiota.

Furthermore, the factors that govern microbiota composition are complex, involving inter-microbial interactions, nutritional and environmental factors like host genetics, diet, age, mode of birth and so on. The gut microbiota also has a great therapeutic potential, but the exact mechanism by gut microbiota could treat many diseases is not well known. It might be because of the change in bacterial compositions. For example, depending on mode of delivery, the neonate may be differentially exposed to maternal or environmental microbes, thereby limiting range of microbes the infant might acquire. Comparison the relationship of these factors and microbial population led to link dysbiosis and the etiology of different pathological conditions. Essential data and studies for the approval still needed to address these points are necessary. To balance these fluctuations may be effective in the treatment of diseases, so continuous studies on the relationship between the intestinal microbiota and the host is also essential. Further investigation will be required to address these issues.

STAR★METHODS

Detailed methods are provided in the online version of this paper and include the following:

- [KEY RESOURCES TABLE](#)
- [RESOURCE AVAILABILITY](#)
 - Lead contact
 - Materials availability
 - Data and code availability
- [EXPERIMENTAL MODEL AND SUBJECT DETAILS](#)
 - Human subjects
 - Mice
 - Cell lines
- [METHOD DETAILS](#)
 - Patients and sample collection
 - DNA extraction and 16S rRNA gene sequencing analysis
 - Mass spectrometry
 - Experimental design and NEC model
 - IEC isolation
 - Western blot analysis
 - IHC staining
 - H&E staining
 - RNA-seq analysis
 - High throughput CUT&Tag
 - ChIP assay
- [QUANTIFICATION AND STATISTICAL ANALYSIS](#)
- [ADDITIONAL RESOURCES](#)

ACKNOWLEDGMENTS

The authors thank Dr. Na Li and Junmei Zhou for technical assistance. This work was supported by the Grant from National Natural Science Foundation of China (No.82001591) and Grant from Shanghai Jiao Tong University (YG2019QNAO1) to Li Lu. This work was also supported by grants from National Natural Science Foundation of China of China to Zhibao Lv (No.82171696) and Shaohua Hu (No.31971163).

AUTHOR CONTRIBUTIONS

T.G: investigation, methodology, visualization, data curation, formal analysis, software, verification of underlying data, writing—original draft. S.H.H.: Investigation, methodology, funding acquisition. W.J.X.: Supervision. J.Z., F.C., T.G.G., W.Q.Q. and F.L.C.: resources. Z.B.L. and L.L.: conceptualization, funding acquisition, project administration, supervision, validation, writing—review & editing. All authors read and approved the final manuscript.

DECLARATION OF INTERESTS

The authors have no financial conflicts of interest.

INCLUSION AND DIVERSITY

We support inclusive, diverse, and equitable conduct of research.

Received: August 25, 2022

Revised: January 7, 2023

Accepted: May 11, 2023

Published: May 14, 2023

REFERENCES

- Lin, P.W., and Stoll, B.J. (2006). Necrotizing enterocolitis. *Lancet* 368, 1271–1283. [https://doi.org/10.1016/S0140-6736\(06\)69525-1](https://doi.org/10.1016/S0140-6736(06)69525-1).
- Gambardella, J., Khondkar, W., Morelli, M.B., Wang, X., Santulli, G., and Trimarco, V. (2020). Arginine and endothelial function. *Biomedicines* 8, 277. <https://doi.org/10.3390/biomedicines8080277>.
- Morris, S.M., Jr. (2016). Arginine metabolism revisited. *J. Nutr.* 146, 2579s–2586s. <https://doi.org/10.3945/jn.115.226621>.
- Wu, G., and Morris, S.M., Jr. (1998). Arginine metabolism: nitric oxide and beyond. *Biochem. J.* 336, 1–17. <https://doi.org/10.1042/bj3360001>.
- Garg, B.D., and Kabra, N.S. (2018). Role of amino acid supplementation in the prevention of necrotizing enterocolitis in preterm neonates - a review of current evidences. *J. Matern. Fetal Neonatal Med.* 31, 2349–2366. <https://doi.org/10.1080/14767058.2017.1342797>.
- Grimble, R.F. (2005). Immunonutrition. *Curr. Opin. Gastroenterol.* 21, 216–222. <https://doi.org/10.1097/01.mog.0000153360.90653.82>.
- Becker, R.M., Wu, G., Galanko, J.A., Chen, W., Maynor, A.R., Bose, C.L., and Rhoads, J.M. (2000). Reduced serum amino acid concentrations in infants with necrotizing enterocolitis. *J. Pediatr.* 137, 785–793. <https://doi.org/10.1067/mpd.2000.109145>.
- Leung, K.T., Chan, K.Y.Y., Ma, T.P.Y., Yu, J.W.S., Tong, J.H.M., Tam, Y.H., Cheung, H.M., To, K.F., Lam, H.S., Lee, K.H., et al. (2016). Dysregulated expression of arginine metabolic enzymes in human intestinal tissues of necrotizing enterocolitis and response of CaCO₂ cells to bacterial components. *J. Nutr. Biochem.* 29, 64–72. <https://doi.org/10.1016/j.jnutbio.2015.10.010>.
- Yazji, I., Sodhi, C.P., Lee, E.K., Good, M., Egan, C.E., Afrazi, A., Neal, M.D., Jia, H., Lin, J., Ma, C., et al. (2013). Endothelial TLR4 activation impairs intestinal microcirculatory perfusion in necrotizing enterocolitis via eNOS-NO-nitrite signaling. *Proc. Natl. Acad. Sci. USA* 110, 9451–9456. <https://doi.org/10.1073/pnas.1219997110>.
- Zhou, W., Li, W., Zheng, X.H., Rong, X., and Huang, L.G. (2014). Glutamine downregulates TLR-2 and TLR-4 expression and protects intestinal tract in preterm neonatal rats with necrotizing enterocolitis. *J. Pediatr. Surg.* 49, 1057–1063. <https://doi.org/10.1016/j.jpedsurg.2014.02.078>.
- Sevastiadou, S., Malamitsi-Puchner, A., Costalos, C., Skouroliakou, M., Briana, D.D., Antsaklis, A., and Roma-Giannikou, E. (2011). The impact of oral glutamine supplementation on the intestinal permeability and incidence of necrotizing enterocolitis/septicemia in premature neonates. *J. Matern. Fetal Neonatal Med.* 24, 1294–1300. <https://doi.org/10.3109/14767058.2011.564240>.
- Bober-Olesińska, K., and Kornacka, M.K. (2005). [Effects of glutamine supplemented parenteral nutrition on the incidence of necrotizing enterocolitis, nosocomial sepsis and length of hospital stay in very low birth weight infants]. *Med. Wieku Rozwoj.* 9, 325–333.
- Frost, B.L., Modi, B.P., Jaksic, T., and Caplan, M.S. (2017). New medical and surgical insights into neonatal necrotizing enterocolitis: a review. *JAMA Pediatr.* 171, 83–88. <https://doi.org/10.1001/jamapediatrics.2016.2708>.
- Cortese, R., Lu, L., Yu, Y., Ruden, D., and Claud, E.C. (2016). Epigenome-Microbiome crosstalk: a potential new paradigm influencing neonatal susceptibility to disease. *Epigenetics* 11, 205–215. <https://doi.org/10.1080/15592294.2016.1155011>.
- Gjaltema, R.A.F., and Rots, M.G. (2020). Advances of epigenetic editing. *Curr. Opin. Chem. Biol.* 57, 75–81. <https://doi.org/10.1016/j.cbpa.2020.04.020>.
- Good, M., Chu, T., Shaw, P., McClain, L., Chamberlain, A., Castro, C., Rimer, J.M., Mihi, B., Gong, Q., Nolan, L.S., et al. (2020). Global hypermethylation of intestinal epithelial cells is a hallmark feature of neonatal surgical necrotizing enterocolitis. *Clin. Epigenet.* 12, 190. <https://doi.org/10.1186/s13148-020-00983-6>.
- Bellanti, J.A. (2020). Epigenetic studies and pediatric research. *Pediatr. Res.* 87, 378–384. <https://doi.org/10.1038/s41390-019-0644-9>.
- Lu, L., Fan, J., Xu, W., Cui, X., Hu, S., Guo, T., and Lv, Z. (2022). DNA methylome mapping identifies epigenetic abnormalities in intestinal lymphocyte regulation in human necrotizing enterocolitis. *Dig. Dis. Sci.* 67, 4434–4443. <https://doi.org/10.1007/s10620-021-07314-6>.
- Wolfson, N.A., Pitcairn, C.A., and Fierke, C.A. (2013). HDAC8 substrates: histones and beyond. *Biopolymers* 99, 112–126. <https://doi.org/10.1002/bip.22135>.
- Chakrabarti, A., Oehme, I., Witt, O., Oliveira, G., Sippl, W., Romier, C., Pierce, R.J., and Jung, M. (2015). HDAC8: a multifaceted target for therapeutic interventions. *Trends Pharmacol. Sci.* 36, 481–492. <https://doi.org/10.1016/j.tips.2015.04.013>.
- Falkenberg, K.J., and Johnstone, R.W. (2014). Histone deacetylases and their inhibitors in cancer, neurological diseases and immune disorders. *Nat. Rev. Drug Discov.* 13, 673–691. <https://doi.org/10.1038/nrd4360>.
- Seto, E., and Yoshida, M. (2014). Erasers of histone acetylation: the histone deacetylase enzymes. *Cold Spring Harbor Perspect. Biol.* 6, a018713. <https://doi.org/10.1101/cshperspect.a018713>.
- Sun, Q., Ji, Y.C., Wang, Z.L., She, X., He, Y., Ai, Q., and Li, L.Q. (2021). Sodium butyrate alleviates intestinal inflammation in mice with necrotizing enterocolitis. *Mediat. Inflamm.* 2021, 6259381. <https://doi.org/10.1155/2021/6259381>.
- He, Y., Du, W., Xiao, S., Zeng, B., She, X., Liu, D., Du, H., Li, L., Li, F., Ai, Q., et al. (2021). Colonization of fecal microbiota from patients with neonatal necrotizing enterocolitis exacerbates intestinal injury in germfree mice subjected to necrotizing enterocolitis-induction protocol via alterations in butyrate and regulatory T cells. *J. Transl. Med.* 19, 510. <https://doi.org/10.1186/s12967-021-03109-5>.
- Candido, E.P., Reeves, R., and Davie, J.R. (1978). Sodium butyrate inhibits histone deacetylation in cultured cells. *Cell* 14, 105–113. [https://doi.org/10.1016/0092-8674\(78\)90305-7](https://doi.org/10.1016/0092-8674(78)90305-7).
- Zhao, T., Kee, H.J., Bai, L., Kim, M.K., Kee, S.J., and Jeong, M.H. (2021). Selective HDAC8 inhibition attenuates isoproterenol-induced cardiac hypertrophy and fibrosis via

- p38 MAPK pathway. *Front. Pharmacol.* 12, 677757. <https://doi.org/10.3389/fphar.2021.677757>.
27. Wu, S.E., Hashimoto-Hill, S., Woo, V., Eshleman, E.M., Whitt, J., Engleman, L., Karns, R., Denson, L.A., Haslam, D.B., and Alenghat, T. (2020). Microbiota-derived metabolite promotes HDAC3 activity in the gut. *Nature* 586, 108–112. <https://doi.org/10.1038/s41586-020-2604-2>.
 28. Whitt, J., Woo, V., Lee, P., Moncivaiz, J., Haberman, Y., Denson, L., Tso, P., and Alenghat, T. (2018). Disruption of epithelial HDAC3 in intestine prevents diet-induced obesity in mice. *Gastroenterology* 155, 501–513. <https://doi.org/10.1053/j.gastro.2018.04.017>.
 29. Lu, L., Fan, J., Xu, W., Cui, X., Hu, S., Guo, T., and Lv, Z. (2021). DNA methylome mapping identifies epigenetic abnormalities in intestinal lymphocyte regulation in human necrotizing enterocolitis. *Dig. Dis. Sci.* <https://doi.org/10.1007/s10620-021-07314-6>.
 30. Sanderson, I.R. (2004). Short chain fatty acid regulation of signaling genes expressed by the intestinal epithelium. *J. Nutr.* 134, 2450S–2454S. <https://doi.org/10.1093/jn/134.9.2450S>.
 31. Zheng, N., Gao, Y., Zhu, W., Meng, D., and Walker, W.A. (2020). Short chain fatty acids produced by colonizing intestinal commensal bacterial interaction with expressed breast milk are anti-inflammatory in human immature enterocytes. *PLoS One* 15, e0229283. <https://doi.org/10.1371/journal.pone.0229283>.
 32. Qin, J., Li, R., Raes, J., Arumugam, M., Burgdorf, K.S., Manichanh, C., Nielsen, T., Pons, N., Levenez, F., Yamada, T., et al. (2010). A human gut microbial gene catalogue established by metagenomic sequencing. *Nature* 464, 59–65. <https://doi.org/10.1038/nature08821>.
 33. Pammi, M., Cope, J., Tarr, P.I., Warner, B.B., Morrow, A.L., Mai, V., Gregory, K.E., Kroll, J.S., McMurtry, V., Ferris, M.J., et al. (2017). Intestinal dysbiosis in preterm infants preceding necrotizing enterocolitis: a systematic review and meta-analysis. *Microbiome* 5, 31. <https://doi.org/10.1186/s40168-017-0248-8>.
 34. Berkhout, D.J.C., Niemarkt, H.J., de Boer, N.K.H., Benninga, M.A., and de Meij, T.G.J. (2018). The potential of gut microbiota and fecal volatile organic compounds analysis as early diagnostic biomarker for necrotizing enterocolitis and sepsis in preterm infants. *Expet Rev. Gastroenterol. Hepatol.* 12, 457–470. <https://doi.org/10.1080/17474124.2018.1446826>.
 35. Morrow, A.L., Lagomarcino, A.J., Schibler, K.R., Taft, D.H., Yu, Z., Wang, B., Altaye, M., Wagner, M., Gevers, D., Ward, D.V., et al. (2013). Early microbial and metabolomic signatures predict later onset of necrotizing enterocolitis in preterm infants. *Microbiome* 1, 13. <https://doi.org/10.1186/2049-2618-1-13>.
 36. Zhou, Y., Shan, G., Sodergren, E., Weinstock, G., Walker, W.A., and Gregory, K.E. (2015). Longitudinal analysis of the premature infant intestinal microbiome prior to necrotizing enterocolitis: a case-control study. *PLoS One* 10, e0118632. <https://doi.org/10.1371/journal.pone.0118632>.
 37. Warner, B.B., Deych, E., Zhou, Y., Hall-Moore, C., Weinstock, G.M., Sodergren, E., Shaikh, N., Hoffmann, J.A., Linneman, L.A., Hamvas, A., et al. (2016). Gut bacteria dysbiosis and necrotizing enterocolitis in very low birthweight infants: a prospective case-control study. *Lancet (London, England)* 387, 1928–1936. [https://doi.org/10.1016/s0140-6736\(16\)00081-7](https://doi.org/10.1016/s0140-6736(16)00081-7).
 38. Krajmalnik-Brown, R., Ilhan, Z.E., Kang, D.W., and DiBaise, J.K. (2012). Effects of gut microbes on nutrient absorption and energy regulation. *Nutr. Clin. Pract.* 27, 201–214. <https://doi.org/10.1177/0884533611436116>.
 39. Neu, J. (2007). Gastrointestinal development and meeting the nutritional needs of premature infants. *Am. J. Clin. Nutr.* 85, 629S–634S. <https://doi.org/10.1093/ajcn/85.2.629S>.
 40. Zhang, D., Tang, Z., Huang, H., Zhou, G., Cui, C., Weng, Y., Liu, W., Kim, S., Lee, S., Perez-Neut, M., et al. (2019). Metabolic regulation of gene expression by histone lactylation. *Nature* 574, 575–580. <https://doi.org/10.1038/s41586-019-1678-1>.
 41. Adam, A.A.A., van der Mark, V.A., Ruiter, J.P.N., Wanders, R.J.A., Oude Elferink, R.P.J., Chamuleau, R., and Hoekstra, R. (2019). Overexpression of carbamoyl-phosphate synthase 1 significantly improves ureagenesis of human liver HepaRG cells only when cultured under shaking conditions. *Mitochondrion* 47, 298–308. <https://doi.org/10.1016/j.mito.2019.02.005>.
 42. Krotova, K., Patel, J.M., Block, E.R., and Zharikov, S. (2010). Hypoxic upregulation of arginase II in human lung endothelial cells. *Am. J. Physiol. Cell Physiol.* 299, C1541–C1548. <https://doi.org/10.1152/ajpcell.00068.2010>.
 43. Walsh, M.C., and Kliegman, R.M. (1986). Necrotizing enterocolitis: treatment based on staging criteria. *Pediatr. Clin.* 33, 179–201. [https://doi.org/10.1016/s0031-3955\(16\)34975-6](https://doi.org/10.1016/s0031-3955(16)34975-6).
 44. Plaisier, S.B., Taschereau, R., Wong, J.A., and Graeber, T.G. (2010). Rank-rank hypergeometric overlap: identification of statistically significant overlap between gene-expression signatures. *Nucleic Acids Res.* 38, e169. <https://doi.org/10.1093/nar/gkq636>.
 45. Kaya-Okur, H.S., Wu, S.J., Codomo, C.A., Pledger, E.S., Bryson, T.D., Henikoff, J.G., Ahmad, K., and Henikoff, S. (2019). CUT&Tag for efficient epigenomic profiling of small samples and single cells. *Nat. Commun.* 10, 1930. <https://doi.org/10.1038/s41467-019-09982-5>.

STAR★METHODS

KEY RESOURCES TABLE

REAGENT or RESOURCE	SOURCE	IDENTIFIER
Antibodies		
HDAC8	ABclonal	Cat# A8865, RRID: AB_2863620
H3K14ac	ABclonal	Cat# A7254
H3K9ac	ABclonal	Cat# A7255
H3K27ac	Cell Signaling Technology	Cat# 8173, RRID: AB_10949503
H4K16ac	ABclonal	Cat# A5280, RRID: AB_2766099
Actin	Cell Signaling Technology	Cat# 4970, RRID: AB_2223172
GFP	ABclonal	Cat# AE012, RRID: AB_2770402
Histone H3	Proteintech	Cat# 17168-1-AP, RRID: AB_2716755
Histone H4	ABclonal	Cat# A1131, RRID: AB_2758500
normal rabbit IgG	Millipore	Cat# 12–370, RRID: AB_145841
normal mouse IgG	Millipore	Cat# 12–371, RRID: AB_145840
rabbit anti-mouse IgG	Abcam	Cat# ab611709
anti-rabbit IgG	Millipore	Cat# AP132, RRID: AB_11214051
Chemicals		
PCI34051	MedChemExpress	Cat# HY-15224
Butyrate	Sigma Aldrich	Cat# 303410
LPS	Sigma Aldrich	Cat# L4524
Esbilac formula	Abbott Laboratories	N/A
TRIzol™ Reagent	Invitrogen	Cat# 15596026
DMEM	Gibco	Cat# 11995065
Penicillin-Streptomycin	Gibco	Cat# 15140-022
Puromycin	Beyotime	Cat# ST551
Fetal Bovine Serum	Gibco	Cat# 10099-141C
Collagenase VIII	Sigma Aldrich	Cat# C2139
DNA Nase I	Sigma Aldrich	Cat# DN25
DTT	Sangon	Cat# B645939
0.5M EDTA	Sangon	Cat# B540625
HEPES	Sangon	Cat# C0215
RIPA buffer	Beyotime	Cat# P0013
Percoll	GE Healthcare Life Sciences	Cat# 17089101
Critical commercial assays		
DNeasy PowerSoil kit	Qiagen	Cat# 12888
SimpleChIP® Plus Sonication	Cell Signaling Technology	Cat# 56383
Chromatin IP Kit		
Hieff UNICON qPCR SYBR	Yeasen	Cat# 11198ES08
Green Master Mix		
EvoM-MLV RT Premix	AG	Cat# AG11706
Deposited data		
RNA-seq data (Figure 3D)	This paper	GSE212694

(Continued on next page)

Continued

REAGENT or RESOURCE	SOURCE	IDENTIFIER
RNA-seq data (Figure 4)	This paper	GSE213187
CUT&Tag data	This paper	GSE213190
Experimental models: Cell lines		
FHs74Int	ATCC	Cat# CCL-241, RRID: CVCL_2899
IEC6	ATCC	Cat# CRL-1592, RRID: CVCL_0343
Experimental models		
Mouse: C57BL/6	Jiesijie Laboratory	Cat# 0653
Software and algorithms		
GraphPad Prism 8	GraphPad	RRID:SCR_002798; http://www.graphpad.com/
Image Lab	Bio-Rad	RRID:SCR_014210; http://www.bio-rad.com/en-us/sku/1709690-image-lab-software
Genescloud	Personalbio	https://www.genescloud.cn
RRHO package ImageJ	R software ImageJ	Version 1.30.0 RRID:SCR_003070; https://imagej.nih.gov/ij/
SPSS 19.0	IBM	RRID:SCR_019096; https://www.ibm.com/products/spss-statistics

RESOURCE AVAILABILITY

Lead contact

Further information and requests for the reagents, please contact and will be fulfilled by the corresponding author Li Lu (luli_2006@126.com).

Materials availability

This study did not generate new unique reagents.

Data and code availability

- This paper analyses existing publicly available data. Data that support the findings of this study are available from GEO (Accession GSE212694, GSE213187, GSE213190) or upon request.
- This paper does not report original code.
- Any additional information required to reanalyze the data reported in this paper is available from the [lead contact](#) upon request.

EXPERIMENTAL MODEL AND SUBJECT DETAILS

Human subjects

A total of 42 preterm infants, excluding those with intestinal malformations and complex malformations, from Shanghai Children's Hospital were enrolled in the study cohort. This study was approved by the ethics committee of Shanghai Children's Hospital (2020RY020-E01) and carried out in accordance with the principles of the Declaration of Helsinki. And each participant gave written informed consent upon recruitment.

Mice

All mice were purchased from Shanghai Jiesijie Laboratory Animal Co., Ltd. The pup mice included two sexes and divided randomly. In order to reduce the influence of environmental factors on the establishment of animal models. All mice kept in a sterile environment with constant temperature and humidity with free access to standard rodent chow and water. All the animal experiments were performed in accordance with the protocol outlined in the Guide for the Care and Use of Laboratory Animals published by the US National Institute of Health and approved by the Animal Care Committee of the Children's Hospital of Shanghai (SHCH-IACUC-2020-XMSB-36). All mice were randomly allocated to the indicated groups.

Cell lines

The non-transformed human fetal intestinal epithelial cell line FHs74Int and the IEC6 cell line were obtained from the American Type Culture Collection (ATCC). FHs74Int cells were cultured in Hybri-Care Medium (ATCC-46X) supplemented with 10% fetal bovine serum (FBS), 1% antibiotic-antimycotic and 30 ng/mL rhEGF. IEC6 cells were cultured in DMEM supplemented with 10% fetal bovine serum and 1% antibiotic-antimycotic. All cells were maintained at 37°C and 5% CO₂.

METHOD DETAILS

Patients and sample collection

The diagnosis of NEC in the infants was based on the presence of clinical criteria—i.e., Bell stage.⁴³ Infants with Bell stage I–III disease were included in the NEC cohort (n = 21), while control samples (n = 21) were chosen based on a similar gestational age, birth weight, sex, and mode of birth of the infants and a similar sampling time. Fecal and serum samples were collected from the 26 preterm infants (Control: n = 13; NEC: n = 13). Fecal and serum samples from NEC patients were collected at the onset of NEC, and the time point of the fecal in the controls group were matched to NEC. Three infants with late-onset NEC (NEC onset at day 71, 95, 101) were harvested in our study. Since the infants in the control group did not stay in the hospital for such a long time, we tried to match the control group who stayed in the hospital for a long time (day 22, 27, 33). And there were no significant differences of sampling time between control and NEC group. The feces and serum were freshly harvested and immediately transported to the laboratory and stored at –80°C for later use.

Intestinal tissues were harvested from the other 16 preterm infants (Control: n = 8; NEC: n = 8) immediately after the operation. Among NEC infants' intestinal samples, resected intestinal tissue samples with inflammatory intestinal tissue around necrosis were collected. For control samples, the two incised ends of surgical intestine of intestinal atresia and stenosis were collected. All samples were collected from the ileum and the ileum proximal to the ileocecal valve was collected into three parts: (1) Part of the intestine was storage in 10% formalin for IHC; (2) Part of the intestine were stored at –80°C for Western blotting and qRT-PCR; (3) Part of the fresh intestine were used to isolate the intestine epithelial cells (IECs).

In this study, we included NEC Bell's stage I for the following two reasons: Firstly, we found that the concentrations of butyric acid were significantly lower in the children with Bell's stage I than in the control during the research. Secondly, infants usually started to take conservative treatment in clinical practice even if they were considered as NEC-I, while the butyrate that we found decreased in stage I may be an effective method for early clinical prevention in the future.

DNA extraction and 16S rRNA gene sequencing analysis

All 26 fecal samples were used to analyze the structure of the microbiome. Total DNA from fecal samples was extracted using a DNeasy PowerSoil kit (Qiagen, Hilden, Germany). DNA concentration and integrity were measured by a NanoDrop 2000 spectrophotometer (Thermo Fisher Scientific, Waltham, MA, USA) and agarose gel electrophoresis, respectively. The V3-V4 variable regions of 16S rRNA genes were amplified with barcoded primers (forward primer: 5'-TACGGRAGGCAGCAG-3'; reverse primer: 5'-AGGGTATC TAATCCT-3'). Water samples subjected to the same DNA extraction and PCR amplification procedures as the fecal samples were used as the controls. Equal amounts of DNA from each sample were pooled and verified using an Agilent 2100 bioanalyzer (Agilent, USA). Sequencing was performed on the Illumina MiSeq platform with two paired-end 300 base pair read cycles (Illumina Inc., San Diego, CA; OE Biotech Company; Shanghai, China).

After sequencing, paired-end reads were preprocessed using Trimmomatic software to detect and cut off ambiguous bases. The paired-end reads were assembled using FLASH software, and the parameters were as follows: 10 bp of minimal overlapping, 200 bp of maximum overlapping and 20% of maximum mismatch rate. Sequences were performed further denoising as follows: reads with ambiguous, homologous sequences or below 200 bp were abandoned. Reads with 75% of bases above Q20 were retained using QIIME software. Then, reads with chimera were detected and removed using VSEARCH. Clean reads were subjected to primer sequences removal and clustering to generate operational taxonomic units (OTUs) using VSEARCH software with 97% similarity cutoff. The representative read of each OTU was

selected using QIIME package. All representative reads were annotated and blasted against Silva database using RDP classifier (confidence threshold was 70%).

Mass spectrometry

Fecal samples from the 13 NEC patients and 13 control patients were used to measure SCFAs concentrations. SCFAs analysis was performed by Shanghai Metabo-Profile Co., Ltd. (China). Fecal pellets (approximately 10 mg) were homogenized with beads in sterile deionized water (25 μ L/sample) for 3 min. Then, 185 μ L of an acetonitrile: methanol (8:2) solution was added to the mixture and centrifuged at 18000 \times g for 20 min. The supernatant was transferred to a 96-well plate. Then, 20 μ L of freshly prepared derivatization reagent was added to each well, and the plate was sealed and placed at 30°C for 60 min of derivatization. Then, 350 μ L of 50% methanol solution prechilled in an ice bath was added to dilute the sample, and the plate was placed at -20°C for 20 min and then centrifuged (4000 \times g, 30 min) at 4°C. Then, 135 μ L of the supernatant was transferred to a new 96-well plate, and 15 μ L of the internal standard was added to each well. The samples were used for analysis by UPLC-MS/MS (ACQUITY UPLC-Xevo TQ-S, Waters Corp., Milford, MA, USA, 2.4).

Serum samples from 26 preterm birth and frozen intestinal samples from mice (n = 3–5 each group, random samples) were used to measure amino acid concentrations. The amino acids of serum were analyzed by professional investigators by methods developed in the clinical laboratory of Shanghai Children's Hospital. Reagents, deuterium-labeled internal standards, standard products, and quality control products were obtained from Guangzhou ClinMeta Medical Device Co., Ltd. Twenty microliters of serum (standard products or quality control products) and 80 μ L of diluted samples were vortexed for 5 min. Ten microliters of diluted serum and 100 μ L of ice-cold methanol containing partial internal standards were vortexed for 5 min. After centrifugation at 13,000 rpm for 5 min, 50 μ L aliquots of the supernatant was placed into autosampler vials and purged with nitrogen until completely dry at 50 degrees. Then, the samples were vortexed after derivatization with 500 μ L of freshly prepared derivatization reagents for 30 min and purged with nitrogen until completely dry after derivatization. These two steps were performed at 60 degrees. Then, 100 μ L aliquots of the dilutions were added to vials and vortexed for 5 min. These vials were mixed well, and 2 μ L was injected onto a separation column (ACE EXCEL 3 AQ, 100 \times 3.0 MM). Sample analysis was performed using LC-MS/MS (Shimadzu LCMS-8040CL). The LCMS-8040CL instrument was operated with the multiple reaction monitoring (MRM) method in positive ion mode to determine the concentrations of all amino acids.

Besides, frozen intestinal samples of mice were homogenized and suspended in a solution with internal standard. After deproteinization and resting, the supernatants were filtered and dehydrated in vacuo. Finally, the supernatant was transferred to an HPLC vial to be used for LC-MS analysis. Prepared supernatant samples were analyzed on an UPLC-MS/MS (ACQUITY UPLC-Xevo TQ-S, Waters Corp., Milford, MA, USA).

Experimental design and NEC model

Firstly, we prepared two litters of C57BL/6 mice at 1 day. At day 5, the mice were divided into the control group (n = 3), NEC group (n = 11). NEC was induced using formula gavage every 4 h for 96 h using 40 μ L of 33% Esbilac formula (Pet-Ag, Abbott Laboratories). Meanwhile, pups were exposed to hypoxia treatments (99.9% N₂ for 100 s), followed by cold stress (4°C for 10 min) every 12 h. The control group were dam-fed without hypoxia and cold stress. All mice were euthanized at 96 h. The ileum was collected into three parts: stored in 10% formalin for HE and IHC; stored at -80°C for qRT-PCR, Western blotting and RNA-sequencing; the remaining fresh intestine for isolating IECs. For the HDAC8 inhibition assay, we purchased six litters of C57BL/6 mice at 1 day every time. At day 4, six litters of C57BL/6 mice were randomly divided into the control group (n = 3), NEC group (n = 10), PCI34051+ NEC group (n = 10), and the residual mice were distributed to PCI34051 group (n = 5–8) in each experiment. For the butyrate acid treatment assay, all neonatal mice at day 5 were randomly divided into the control group (n = 3), NEC group (n = 10), NEC + butyrate group (n = 10), and the residual mice were distributed to butyrate group (n = 3–7) in each experiment. NEC model was constructed as above. The control and PCI34051 group or butyrate group were dam-fed without hypoxia and cold stress. In the PCI34051 and PCI34051-treated NEC group, the PCI34051 was fed with a volume of 10 mg/kg body weight since day 4 to day 8. In the butyrate and butyrate-treated NEC group, the butyrate (150 mM) was fed once at a volume of 30 μ L/g body weight since the second day to the end. At the same time, the mice in the other groups were fed with the equal volume of

PBS. All animals were euthanized after 96 h when NEC modeling finished. Three independent experiments were performed.

The ileum was collected into three parts: stored in 10% formalin for HE and IHC; stored at 80°C for qRT-PCR, Western blotting, RNA-sequencing and amino acid measurement; the remaining fresh intestine used for isolating IECs.

IEC isolation

The intestine tissues were collected from the patients and mice. Firstly, fat tissues of the small intestines were removed. Then the tissues were cut longitudinally and rinsed thoroughly with ice-cold PBS to remove luminal contents including feces. The rinsed tissues transferred to a digestion solution including 1 mM DTT, 30 mM EDTA and 10 mM HEPES and placed in a constant temperature shaker at 200rpm, 37°C for 10 min. After that, transferred the intestine into a digestion buffer including 30 mM EDTA and 10 mM HEPES and incubated at 37°C, 200rpm, for 10min. Then pass the solution through 70um cell strainer to remove tissue fragments. The filtered cell suspensions were applied to Percoll (GE Healthcare Life Sciences, USA) density gradients (25%/40%/75%). After centrifugation at 4°C, 2000 × g for 20 min, the interface between the 25% and 40% layers was collected to obtain IECs. The IECs were collected and stored at – 80°C until subsequent use.

Western blot analysis

For lysate preparation, cells were lysed in radioimmunoprecipitation assay (RIPA) buffer for 30 min. Protein concentrations of samples were determined using a bicinchoninic acid (BCA) protein assay kit. After centrifugation, lysates were resolved on sodium dodecyl sulfate polyacrylamide gel electrophoresis (SDS-PAGE) and then transferred to a polyvinylidene difluoride (PVDF) membrane (Millipore). The blots were blocked in 5% milk for 1 hour at room temperature. Next, PVDF membranes were incubated overnight at 4°C with primary antibodies or secondary antibodies in 5% milk for 2 hours. Then, the membranes were developed using Immobilon Western Detection Reagents.

IHC staining

For immunohistochemical staining, 6-μm-thick paraffin-embedded sections were dewaxed in xylene and rehydrated through gradient alcohols (100, 90, 80 and 75%). After peroxidase activity was blocked using 3% H₂O₂ in methanol for 15 min at room temperature. Antigen retrieval of tissue sections was performed by sodium citrate buffer. Sections were washed three times with PBS and blocked with 5% bovine serum albumin for 60 min at room temperature. Sections were incubated overnight at 4°C with primary antibodies, followed by incubation with horseradish peroxidase (HRP)-coupled secondary antibodies at room temperature for 1 h. The color was developed by a 15 min incubation at room temperature with DAB solution, and then. The blue nucleus was stained by hematoxylin solution. Finally, the sheets were blocked with neutral balsam.

H&E staining

Fresh proximal ileocecum samples were immediately fixed in 4% paraformaldehyde. Then, the sections were dehydrated, embedded in paraffin. The embedded ileocecal intestinal tissue was sliced at a thickness of 6 μm, and stained with hematoxylin and eosin, and sealed. The histopathological changes in the intestine were observed under an optical microscope. The diagnosis of NEC was performed by changes in intestinal tissue with double-blind observational method in this study. NEC was scored based on the severity of the damage from the mucosa to the lamina propria as follows: Grade 0, no damage; Grade 1, mild separation or edema; Grade 2, moderate separation or edema; Grade 3, necrosis of the entire villus; 4, total destructions of the intestinal epithelium. A pathological score ≥ 2 was considered positive for NEC.

RNA-seq analysis

The mRNA libraries were constructed from intestinal tissue (Control, NEC / Control, NEC, PCI34051, PCI34051+NEC). Sequencing was performed by Shanghai Jiayin Biotechnology Co., Ltd. (China). Total RNA was extracted using TRIzol reagent (Invitrogen, Carlsbad, CA) and chloroform, and RNA integrity was assessed using an RNA Nano 6000 Assay Kit for the Agilent Bioanalyzer 2100 system (Agilent Technologies, CA, USA). mRNA sequencing libraries were generated using an NEBNext® Ultra™ RNA Library Prep Kit for Illumina® (NEB, USA) following the manufacturer's recommendations, and index codes were

added to attribute sequences to each sample. Clustering of the index-coded samples was performed on a cBot Cluster Generation System using a TruSeq PE Cluster Kit v3-cBot-HS (Illumina) according to the manufacturer's instructions. After cluster generation, the library preparations were sequenced on the Illumina NovaSeq platform, and 150 bp paired-end reads were generated.

For analysis, all the downstream analyses were based on the clean data. Qualified reads were aligned to mm10 mouse genome using STAR. HTSeq v0.6.0 was used to calculate counts and fragments mapped to each gene. The R package DESeq2 was used to filter differential gene expression. The mRNAs with p -value < 0.05 and fold change > 1 were defined as significant DEmRNAs. To assess the functions of the DEmRNAs, Gene Ontology (GO) and Kyoto Encyclopedia of Genes and Genomes (KEGG) pathway enrichment analyses were performed using DAVID. RRHO analysis was performed to assess degree of overlap in gene signatures across intestine regions in NEC vs control group and PCI34051+NEC vs NEC group directly. The analysis were performed with RRHO package (Version 1.30.0) in R software (Version 4.0.3) carrying out as described in previous research.⁴⁴ The downregulated genes in NEC vs control group and up-regulated genes in PCI34051+NEC vs NEC group were marked as the same direction (signed -1), while upregulated genes in NEC vs control group and downregulated genes in PCI34051+NEC vs NEC group were marked as the same direction (signed 1).

High throughput CUT&Tag

Cleavage under targets and tagmentation (CUT&Tag) assays were performed by Shanghai Jiayin Biotechnology Co., Ltd. (China) as described previously.⁴⁵ Briefly, 1×10^5 cells were washed twice gently with wash buffer (20 mM HEPES, pH 7.5; 150 mM NaCl; 0.5 mM spermidine; and $1 \times$ protease inhibitor cocktail). Ten microliters of concanavalin A-coated magnetic beads (Bangs Laboratories) were added to each sample and incubated at RT for 10 minutes. Unbound supernatant was removed, and bead-bound cells were resuspended with Dig wash buffer (20 mM HEPES, pH 7.5; 150 mM NaCl; 0.5 mM spermidine; $1 \times$ protease inhibitor cocktail; 0.05% digitonin; and 2 mM EDTA) and a 1:50 dilution of primary antibody or control IgG (normal rabbit IgG: Millipore cat. no. 12–370, normal mouse IgG: Millipore cat. 12–371) and were then incubated on a rotating platform overnight at 4°C . The primary antibody was removed using a magnetic stand. A secondary antibody (rabbit anti-mouse IgG H&L: Abcam, ab611709; anti-rabbit IgG, goat monoclonal: Millipore AP132) was diluted 1:100 in Dig wash buffer and incubated with the cells at RT for 60 min. The cells were washed 2–3 times in Dig wash buffer using a magnetic stand. A 1:100 dilution of the pA-Tn5 adapter complex was prepared in Dig-med buffer (0.01% digitonin; 20 mM HEPES, pH 7.5; 300 mM NaCl; 0.5 mM spermidine; and $1 \times$ protease inhibitor cocktail) and incubated with the cells at RT for 1 hour. The cells were washed 2–3 \times for 5 min each in 1 mL of Dig-med buffer. Then, the cells were resuspended in tagmentation buffer (10 mM MgCl₂ in Dig-med buffer) and incubated at 37°C for 1 h. DNA was purified using phenol–chloroform–isoamyl alcohol extraction and ethanol precipitation.

To amplify libraries, 21 μL of DNA was mixed with 2 μL of a universal i5 primer and a uniquely barcoded i7 primer. A 25 μL volume of NEB Next HiFi 2 \times PCR Master Mix was added and mixed. The sample was placed in a thermal cycler with a heated lid, and amplification was performed using the following thermal cycling conditions: 72°C for 5 min (gap repair); 98°C for 30 s; 14 cycles at 98°C for 10 s and 63°C for 30 s; final extension at 72°C for 1 min; and holding at 8°C . Library clean-up was performed with XP beads (Beckman Counter). The size distribution of the libraries was determined with an Agilent 4200 TapeStation, and libraries were mixed to achieve equal representation as desired, aiming for the final concentration recommended by the manufacturer. Sequencing was performed on the Illumina NovaSeq 6000 platform with 150 bp paired-end reads following the manufacturer's instructions.

After quality control, the reads were then aligned to hg38 genome. Peak calling was performed using MACS2 software with a cut-off q value < 0.05 . Peaks were annotated by ChIPseeker package. Differential peaks were assessed with DESeq2 ($|\text{fold change}| \geq 2$, p -value < 0.05). H3K9ac signals in chromosomes were visualized using IGV. The whole CUT&Tag data are available in the GEO database at the accession number GSE213190.

ChIP assay

The ChIP assay was performed using a SimpleChIP® Plus Sonication Chromatin IP Kit (#56383, Cell Signaling Technology). Briefly, cells were first crosslinked with formaldehyde (1% final) for 10 min. After

being incubated with glycine for 5 min at room temperature and washed three times with PBS. Cells were scraped to harvest cell pellets. The nucleic fraction was isolated from the cell lysate by resuspending separately with the ChIP Sonication Cell Lysis Buffer and ChIP Sonication Nuclear Lysis Buffer. After being fragmented via sonication, the chromatin was incubated with H3K9ac (5 µg per reaction) or IgG for 4 h at 4°C with rotation. Then, the ChIP-Grade Protein G beads were added to each immunoprecipitation reaction and incubated for another 2 h at 4°C with rotation. The captured protein-DNA was then de-crosslinked using 5 M NaCl and Proteinase K for 2 h at 65°C. Finally, DNA was purified with spin columns and analyzed by qPCR. DNA (2%) of each sample served as input fraction.

QUANTIFICATION AND STATISTICAL ANALYSIS

Statistical calculations were carried out using SPSS 19.0. Statistical comparisons between only two groups were carried out by Student's t test, but the Mann-Whitney test was used if the data were nonnormally distributed. One-way analysis of variance (ANOVA) followed by Dunnett's T3 or Tukey's post hoc test was used for multiple-group comparisons. The relationship between microbial community structure and butyric acid in NEC and the relationship between amino acids and SCFAs were examined using the Pearson correlation analysis. Statistically significant differences were defined as $p < 0.05$ (*), $p < 0.01$ (**), and $p < 0.001$ (***)

ADDITIONAL RESOURCES

The clinical trial was registered on Chinese Clinical Trial Registry with the registration numbers ChiCTR2100043104 (weblinks <https://www.chictr.org.cn/showproj.html>).